

Final Draft
of the original manuscript:

Gandra, J.; Krohn, H.; Miranda, R.M.; Vilaca, P.; Quintino, L.; dos Santos, J.F.:
Friction surfacing - A review
In: Journal of Materials Processing Technology (2013) Elsevier

DOI: 10.1016/j.jmatprotec.2013.12.008

Friction surfacing - a review

J. Gandra^a, H. Krohn^b, R.M. Miranda^c, P. Vilaça^d, L. Coutinho^a, J.F. dos Santos^b

^a *Instituto Superior Técnico, Universidade Técnica de Lisboa, Av. Rovisco Pais 1, 1049-001 Lisboa, Portugal*

^b *Helmholtz-Zentrum Geesthacht GmbH, Institute of Materials Research, Materials Mechanics, Solid State Joining Processes (WMP), Max-Planck-St. 1, D-21502 Geesthacht, Germany*

^c *DEMI, Faculdade de Ciências e Tecnologia, Universidade Nova de Lisboa, 2829-516 Caparica, Portugal*

^d *Department of Engineering Design and Production, School of Engineering, Aalto University, P.O. Box 1420, FI-00076 Aalto, Finland*

Abstract

Friction surfacing (FS) is a solid state technology with increasing applications in the context of localized surface engineering. FS has been investigated mainly for producing fine grained coatings, which exhibit superior wear and corrosion properties. Since no bulk melting takes place, this process allows the dissimilar joining of materials that would be otherwise incompatible or difficult to deposit by fusion based methods.

Several studies also emphasize its energy efficiency and low environmental impact as key advantages when compared with other alternative technologies. Main applications include the repair of worn or damaged surfaces through building up or crack sealing. It has also been applied to enhance surface properties at specific areas in the manufacturing of parts and tools. A wide range of materials combinations has been deposited by FS, mainly alloy and stainless steels. Aluminium, magnesium and titanium alloys have also been investigated, including the production of metal matrix composites.

Starting with a brief introduction, this review presents a detailed description of the thermo-mechanical and microstructural transformations, as well as, process modelling approaches. The material combinations investigated so far and the effect of process parameters are also addressed. An overview of the main technologic and equipment

advances is presented, including: computational optimization models, surface preparation, gas protection, post-processing methods, pre-heating and cooling. An assessment of the material deposition rate and the specific energy consumption is also provided, comparing friction surfacing to mainstream electric arc, laser and thermal spraying based processes. Based on current process advantages and disadvantages, an outlook on future research and development is provided.

Friction surfacing has a significant potential for further industrial applications and is being developed as a practicable alternative to mainstream coating processes. The present review paper provides a broad overview throughout the fundamentals of FS and the most relevant technology developments, establishing both a theoretical and technical basis for new researchers and industrial practitioners searching for new coating alternatives.

Keywords: Friction surfacing, Metal deposition, Coating, Solid state processing.

Contents

1. Introduction	6
2. Thermo-mechanical process.....	8
2.1. Microstructural evolution	14
2.1.1. Steels.....	14
2.1.2. Aluminium and magnesium alloys	19
2.1.3. Titanium alloys	23
2.1.4. NiAl Bronze.....	24
2.2. Joining mechanisms	25
3. Process parameters	33
3.1. Equipment and control.....	33
3.2. Influence of process parameters	37
3.2.1. Axial force	38
3.2.2. Rotation speed	39
3.2.3. Travel speed.....	40
3.2.4. Consumable rod diameter	43
4. Process modelling	47
5. Configurations and designs	56
6. Technology developments.....	63
6.1. Consumable rod support systems	63
6.2. Pre-heating or cooling concepts.....	63
6.3. Shielding gas.....	66
6.4. Flash cutting concepts.....	66
6.5. Preparation and post-processing	66
6.6. Composite production.....	69
7. Advantages and disadvantages.....	71
8. Performance analysis.....	73
8.1. Material transfer.....	74
8.2. Energy consumption	75
9. Case studies and industrial applications.....	76
10. Summary and future outlook	80

1. Introduction

Friction surfacing (FS) is a solid state coating process based on the plastic deformation of a metallic consumable rod. As depicted in Fig. 1a, a rotating rod is pressed against the substrate under an applied axial load (Fig. 1b). Frictional heat generates a viscoplastic boundary layer at the rod tip. The pressure and temperature conditions lead to an interdiffusion process resulting in a metallic bond between the plasticised material and the substrate. Heat conduction into the substrate enables this layer to consolidate near the bonded interface, and as such, the viscoplastic shearing interface is formed between the rotating consumable rod and the deposited layer. With the on-going heat conduction, this viscoplastic shearing interface moves away from the substrate surface, increasing the thickness of the layer (Fig. 1c). By applying a travelling movement, the viscoplastic material is deposited onto the substrate surface in a continuous process (Fig. 1d). Note that FS relies solely on interfacial friction and plastic deformation for heat source, allowing to process materials at temperatures below fusion. Given the thermo-mechanical process experienced, a continuous layer of fine grained microstructures is deposited, from the progressive consumption of the rod. The process is also known by the generation of a revolving flash of material at the rod tip, giving it a characteristic mushroom-shaped geometry.

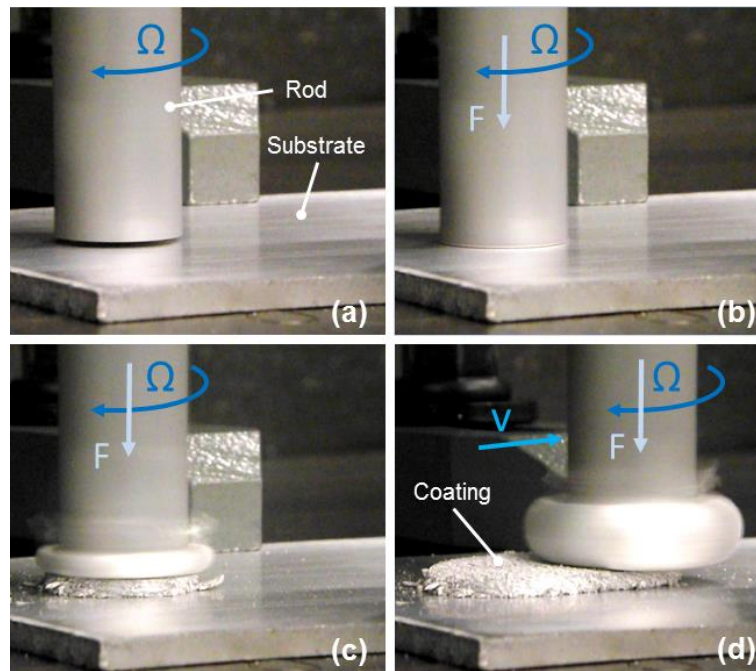


Fig. 1. Friction surfacing of an AA6082-T6 aluminium alloy over AA2024-T3. (a) Rotation start, (b) initial contact, (c) initial deformation stage and (d) deposition stage.

Considered as a variant of Friction Welding by Nicholas (1993), the original FS concept was first mentioned in a patent by Klopstock and Neelands (1941). Although some reports summarized by Bishop (1960) indicate that the process was also developed during the 50s in the USSR, research addressing FS remained relatively dormant in the following decades. Since the late 80s, a new focus was drawn onto the process, following the growing interest on friction-based solid state processes (Nicholas, 2003). In a search for superior coating solutions, FS has been investigated mainly for producing homogeneous fine grained coatings, which exhibit superior wear or corrosion properties (Nicholas, 1993). First application case studies addressed the rehabilitation of worn or damaged parts through building up or crack sealing in localized areas, as proposed by Dunkerton and Thomas (1984).

The process allows the deposition of materials containing hard phases, which cannot be easily formed, such as, tool steels and Co-basis alloys. Nicholas (2003) emphasised that

since no bulk melting takes place during the coating process, it is possible to join dissimilar materials that would be otherwise incompatible or are difficult to deposit by fusion based methods. Similar to other friction-based joining and processing technologies, the lower heat input reduces the heat affection of the base material microstructures, avoiding the degradation of material properties (Thomas et al., 2002). As stated by Bedford and Richards (1985), the absence of melting also results in the absence of dilution, as well as, lower residual stress levels since solidification shrinkage does not occur. A wide range of materials combinations has been deposited by FS, mainly tool steels, stainless steels, mild steel, copper and nickel-based alloys. Alloys such as aluminium, magnesium and titanium have also been investigated, as well as, metal matrix composites.

Although FS is not considered as a new technology, the demand for superior coating solutions drives the on-going interest from the scientific community, making it a still emerging alternative process.

2. Thermo-mechanical process

FS involves a high complexity of transformations, combining both hot-working and joining principles. As other friction based manufacturing technologies, a viscoplasticized solid state region is generated and processed into a new shape and metallurgical condition. Although this region remains in solid state, it presents a three-dimensional material flow pattern that enables the joining between different materials. This phenomenon is generally referred to as the “third-body region” concept, as described by Thomas (2009b). This “third-body region” is characterized by a relatively low flow stress and temperatures above the recrystallization temperature but below the melting temperature of the material. Being driven exclusively by the introduction of

mechanical energy, the heat is generated by friction dissipation during deformation at contacting interfaces and internally by the consumable rod material flow.

Because the heat generated by friction dissipation tends to zero as the material gets near the fusion temperature the maximum temperature achieved within processed zone is physically limited by the fusion temperature and thus all the deformation is restricted to solid state condition. Therefore a metal cannot reach fusion solely by plastic deformation on its own.

As reported by Rafi et al. (2011a), the frictional heat is conducted along the consumable rod, establishing a temperature gradient that determines the level of deformation. As proposed by Bedford et al. (2001), it is based on such a gradient that the material gradually softens and plastically deformed in a torsion/compression process by the colder material above (Fig. 2). Additionally, Fukakusa (1996) proposed that the material in FS is transferred along a rotational contact plane along which slippage occurs between the rotating consumable rod and the deposited layer. Also referred to as a rubbing interface by Bedford et al. (2001), this contact plane is developed during the plasticizing stage at the initial stages of the process, mainly due to the contact and subsequent joining of the viscoplastic material to the substrate. The speed difference between the rotating consumable rod and the deposited layer promotes this viscous slipping. The distance of such contact plane to the substrate surface will determine the thickness of the coating produced (Bedford, 1991). The viscous shearing at this interface is considered to be one most significant heat sources in the process, as is also described by Gandra et al. (2012). As the rotating consumable travels, the material at the rubbing interface will either go towards developing flash or it will be transferred onto the substrate in a rolling fashion, cooling and producing a bond.

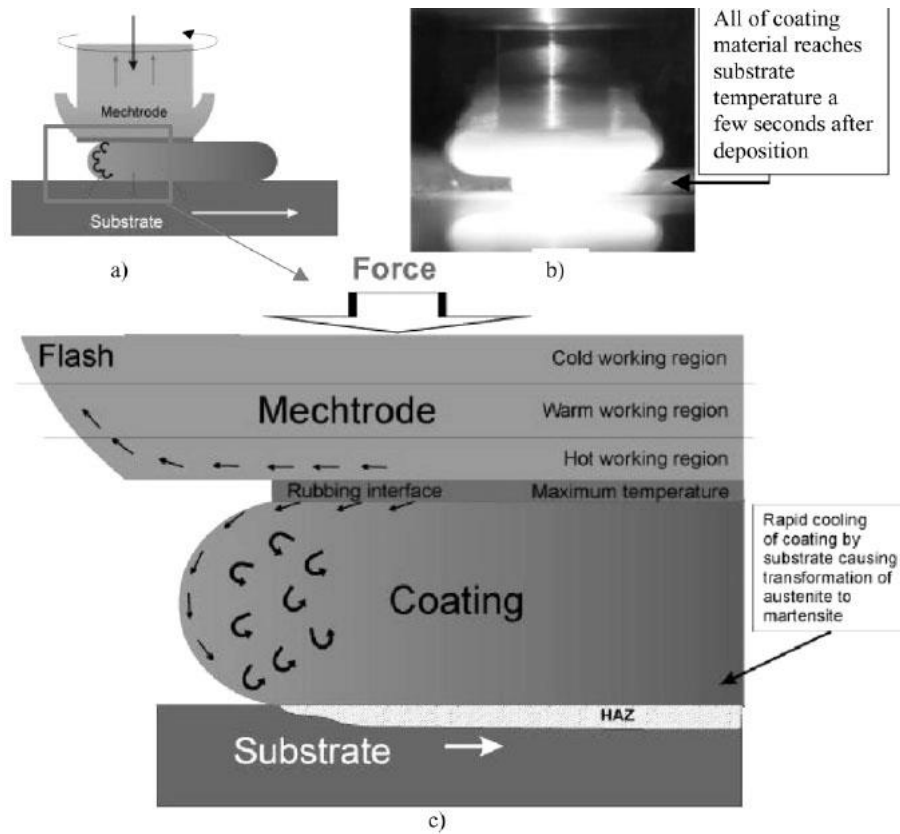


Fig. 2. Thermo-mechanical events in the FS of high speed steels (Bedford et al., 2001).

In FS, the “third-body region” is not fully constrained. The highly plasticized material at the tip of the consumable rod is pressed against the substrate without lateral restraint, flowing outside the consumable rod diameter region. This promotes the development of a revolving flash, as well as, the lack of bonding at the coating edges on both the advancing (rotation and travel movements are in the same direction) and retreating sides (rotation and substrate movement are in opposite directions), as described by Nicholas and Thomas (1986). Hence, the fully bonded width of the deposits produced by FS is typically less than the diameter of the consumable, as reported by Nicholas (1993). Fig. 3 shows cross section micrographs of an AISI 316 stainless steel deposit over a mild steel substrate. Fig. 3a presents a fully bonded interface at the cross section centre, while Fig. 3b shows the edge of the coating, frequently referred as the undercut region by Vitanov et al. (2000). Nevertheless, flash and unbounded edges play an important role, providing

temperature and pressure boundary conditions for the joining process, as was evidenced by Vilaça et al. (2012).

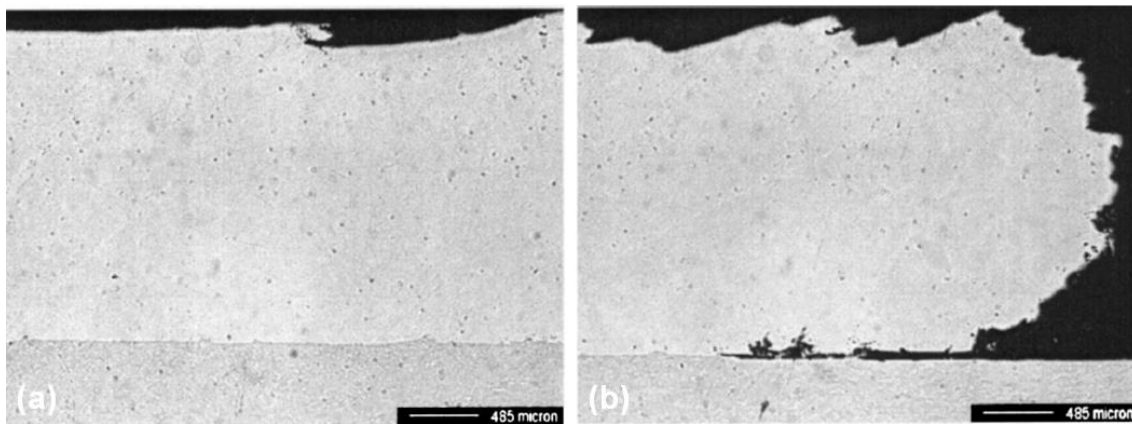


Fig. 3. Cross-section showing coating/substrate interface. FS of AISI 316 stainless steel on a mild steel substrate. (a) Fully bonded interface at coating center, (b) undercut region at the coating edge (Vitanov et al., 2000).

Typical FS coatings for several material combinations are shown in Fig. 4. The top surface of the coating presents ripple-like features, which is an inherent characteristic of the process. Surface roughness and ripple formation are related to the nature of material transfer. According to Bedford et al. (2001), the plasticized metal is transferred in discrete layers of elliptical shape and each layer gets deposited one after the other with a small offset, based on the ratio between rod rotation and travel speeds. This periodic revolving layer deposition phenomenon was also described by Batchelor et al. (1996) and Sakihama et al. (2003), in the deposition of both ferrous and aluminium alloys. From Fig. 4, it can also be seen that the deposit edge on the advancing side is smoother and straight. In contrast, the deposit edge on the retreating side is uneven with a ragged appearance (Rafi et al., 2010a).

Rafi et al. (2010b) observed that the depositions usually present an offset from the centre of the consumable rod, towards the advancing side, as shown in Fig. 4a. This

offset is related with the combined effect of rotation and travel speed on the advancing side, as is reported by Gandra et al. (2013a) in the deposition of AA6082-T6 over AA2024-T3. In the FS of AA5052 aluminium alloy, thermocouple measurements reported by Sakihama et al. (2003) have shown that the advancing side reaches higher temperatures than the retreating side in about 52 K, which is consistent with the coating offset towards this particular side.

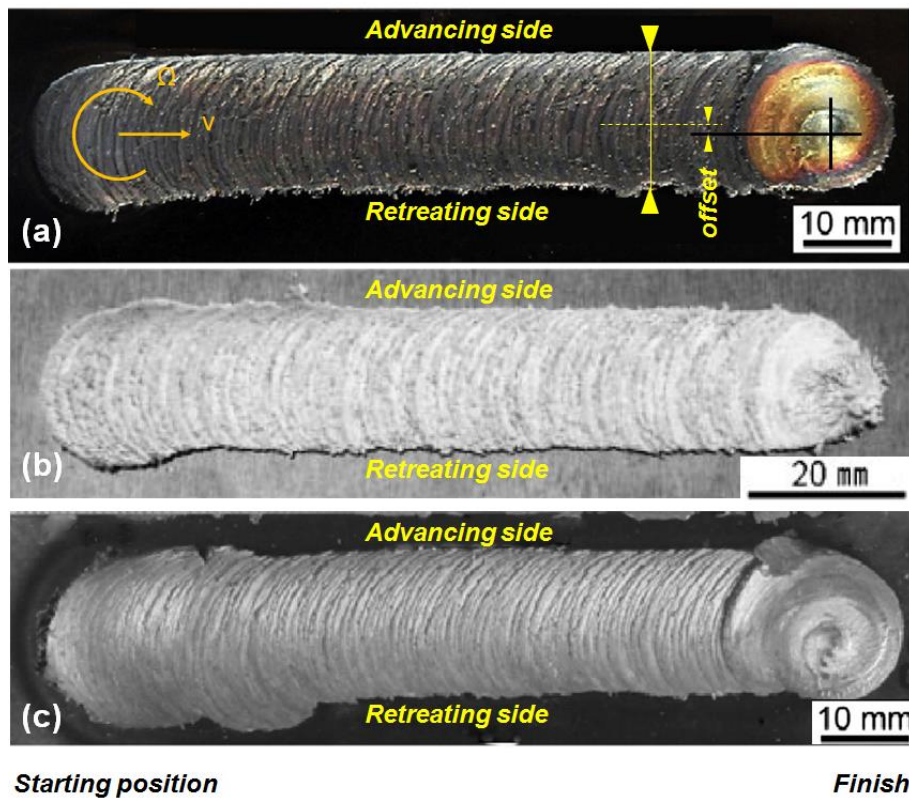


Fig. 4. Typical top view of FS deposits. (a) AISI H13 over AISI 1020 (Rafi et al., 2010a), (b) AA2017 over AA5052 (Tokisue et al., 2006), (c) AISI 310 over AISI 1020 (Rafi et al., 2010b).

By extracting the consumable during the deposition stage it is possible to observe the deposition process, as shown in Fig. 5 in the deposition of mild steel over mild steel reported by Gandra et al. (2012). This analysis suggests that the material is not transferred strictly along a vertical direction, as there is a contribution from rotation and travel speeds. Plastic deformation of the substrate evidences that the consumable

material is rubbed against it from the advancing to the retreating side, fully bonding at the back of the rod, from the retreating to the advancing side.

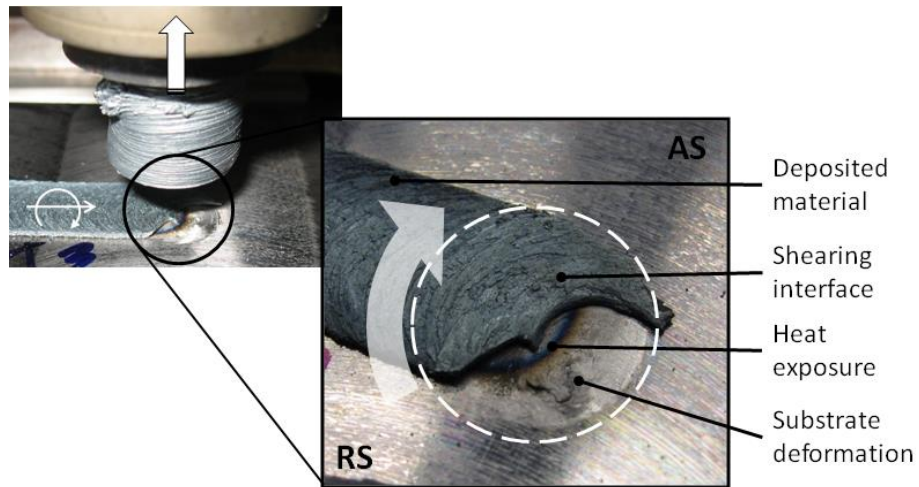


Fig. 5. Deposition process of mild steel over mild steel. Nomenclature: AS - advancing side, RS - retreating side (Gandra et al., 2012).

Similar conclusions regarding the study of material flow in FS were presented by Rafi et al. (2011b) using a tracer technique. The AISI 304 stainless steel consumable rods were loaded with tungsten powder tracers using 3 mm diameter holes drilled in several configurations. Top X-ray radiograph evidenced the tracer distribution, suggesting that the material is transferred from the advancing side to the retreating side, as presented in Fig. 6. A recirculation of material can be observed at the retreating side.

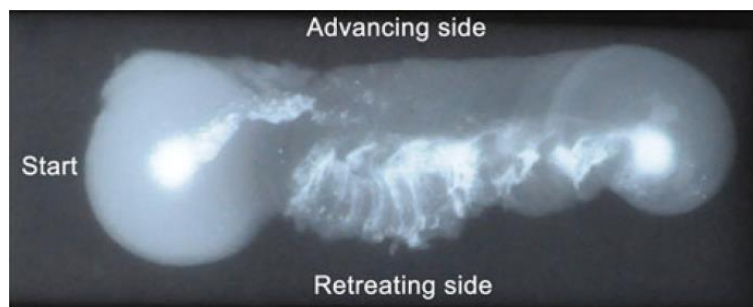


Fig. 6. Study of material flow in FS using a tracer marking technique. Top view X-ray radiographs revealing tracer distribution. Hole filled with tracers was placed at rod centre (Rafi et al., 2011b).

Fukakusa (1996) also studied the plastic flow in FS using a tracer technique. The consumable rods consisted of a AISI 304 portion inserted within a hollow AISI 403 rod. This composite assembly enabled to trace the material flow and to study the material deposition phenomenon. The authors determined that the deposited material was provided mostly by the centre of the rod, while the metal at the periphery formed the flash.

Despite the asymmetric nature of the material transfer process, no significant microstructural or material property differences between advancing and retreating sides are observed, as reported by Rafi et al. (2011c).

2.1. Microstructural evolution

As described in the previous section, FS relies on processing of the material into a viscoplastic state, which implies its dynamic recrystallization. Upon deposition, cooling occurs by the convection to the surrounding environment and conduction into the substrate. As reported by Bedford et al. (2001) such cooling process can occur within seconds, thereby producing a fine grain and homogeneous coating. Depending on the consumable rod material chemical composition, other transformations can arise from the thermal effects experienced during FS, namely phase transformations or modification of the distribution of the second phase particles.

2.1.1. Steels

The FS of steels alloys involves full austenization, as the phase transformation of iron from body centre cubic (BCC) to face centre cubic (FCC) is required to achieve a viscoplastic state. Apart for the grain refinement due to dynamic recrystallization, the coating hardening will be determined by quenching, depending on the carbon content, alloying composition and cooling rate. Additionally, second phase particles can be

dissolved during deformation. After cooling the alloying elements can either remain in solid solution or re-precipitate in a fine dispersion of second phase particles.

One of the most relevant studies addressing these transformations was presented by Bedford et al. (2001). The authors studied the thermo-mechanical events experienced by the consumable rod material and the substrate in the FS of high-speed steels, such as, BM2, BT15 and ASP30 onto plain carbon steel plates. The material at the rubbing interface was seen to experience temperatures close to 1020°C, enabling full austenitization and carbide dissolution. A cooling rate of about 400 °C/s triggered the martensitic transformation within a few seconds of deposition. The magnitude of grain refinement also suggested some other effects, namely the fracture of carbides and a mechanical refinement of the austenite grains. A 0.5 mm deep substrate heat affected zone (HAZ) was observed. The high-speed steel deposits presented a fine and homogeneously distributed carbides in the fully hardened state.

The effect on how FS leads to transformation into fine martensitic microstructures was also described by Rafi et al. (2011c) in the FS of AISI H13 hot work tool steel over mild steel substrates. Since the consumable rod microstructure presented a large number of carbide particles (Fig. 7a), their absence in the coating suggests dissolution during austenitization. The fast cooling rate experienced prevented re-precipitation. Coatings exhibited a fine equiaxial and homogeneous martensitic microstructure (Fig. 7b), with hardness values up to 740 HV, which presents a 190% hardness increase in comparison with the original rod condition (Fig. 7a). Consumable rod grain structure was refined from 50-60 µm to 2-10 µm during deposition. Fig. 8 shows the microhardness profile along the interface from the coating surface to the unaffected substrate. Hardness is higher at the coating surface and the interface, as grain size gradients were observed

along the main directions of heat dissipation (conduction to the substrate and convection at the coating surface).

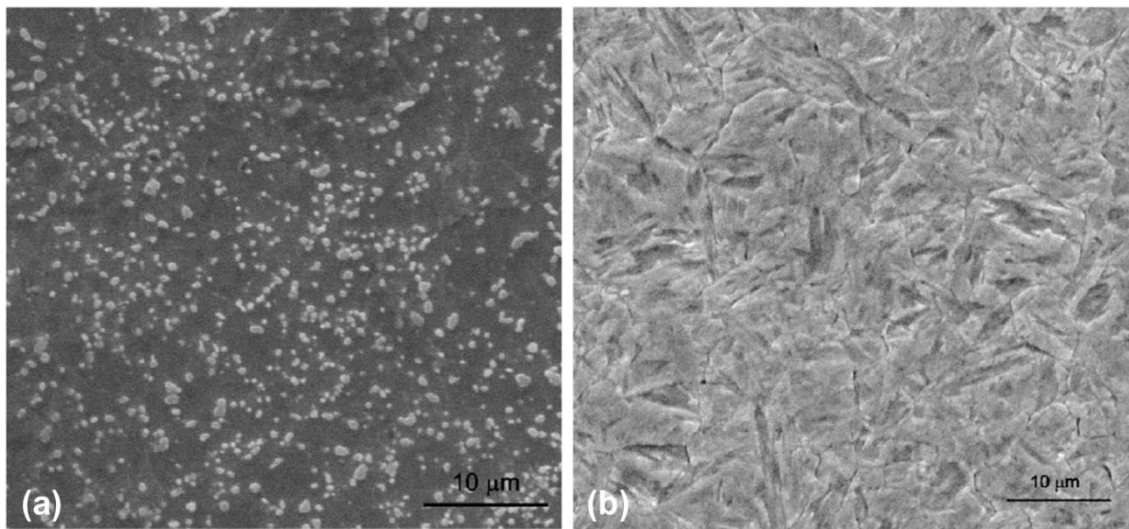


Fig. 7. Comparison between (a) the AISI H13 original rod microstructure and (b) the as-deposited condition, provided by SEM analysis. FS of AISI H13 tool steel over mild steel (Rafi et al., 2010a).

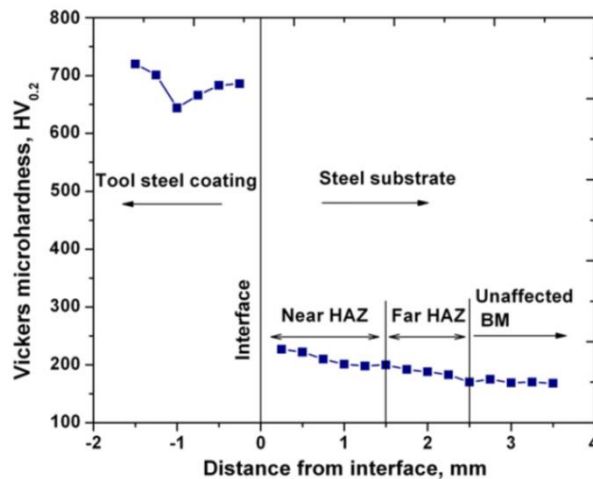


Fig. 8. Vickers microhardness profile across the coating/substrate interface (Rafi et al., 2011c).

Rao et al. (2012a) reported some mechanical effects on the carbide distribution in the FS of Stellite6 over mild steel, such as their fragmentation into finer particles as a consequence of the bulk plastic deformation of the consumable rod. Kramer de Macedo et al. (2010) studied the viability of recovering components in ABNT 1070 high carbon

steel using consumable rods of ABNT 8620, ABNT 4140 and austenitic stainless steel AISI 310. The deposits presented hardness values of 500, 680 and 200 HV, respectively. The substrate HAZ presented hardness values from 800 to 900 HV across a 1.5 mm depth, as its high carbon content enabled the generation of predominantly martensitic microstructures. The unaltered substrate had a 300 HV hardness.

Puli and Janaki Ram (2012b) addressed the microstructural transformations in the FS of a martensitic stainless steel AISI 440C over mild steel. Infrared thermography revealed a maximum temperature of 1150 °C, which resulted in the transformation of ferrite to austenite and dissolution of some of the $M_{23}C_6$ carbides during the heating stage. The severe plastic deformation involved was also presumed to cause fragmentation of coarser carbide particles. Hence, the material as it gets deposited consists of austenite with some undissolved $M_{23}C_6$ carbides. After deposition, the coating cooled to 300 °C, during approximately 10 seconds, resulting in a martensitic microstructure with retained austenite, with both coarse and fine $M_{23}C_6$ carbides (Fig. 9). Some carbide re-precipitation is also expected. The coatings presented a hardness of approximately 590 HV. Further work on the FS of martensitic stainless steels was presented by Puli et al. (2011), with special emphasis on bend and shear testing.

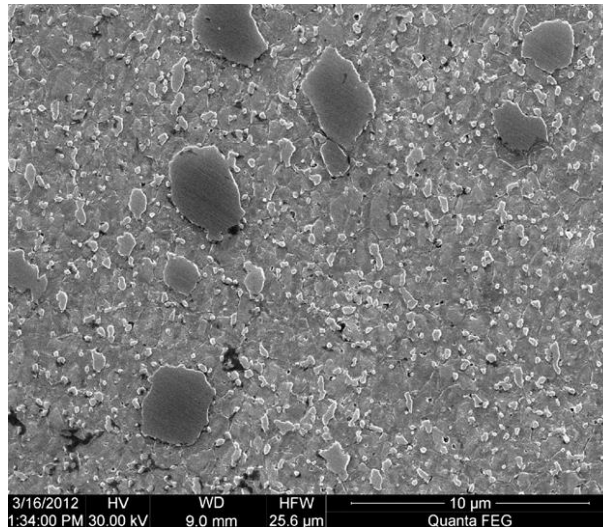


Fig. 9. SEM observation of AISI 440C coating microstructure (Puli and Janaki Ram, 2012b).

In the deposition of austenitic stainless steel AISI316L over mild steel, Puli and Janaki Ram (2012a) reported a coating grain size of fine-grained wrought microstructure with an average grain size of $9 \pm 3 \mu\text{m}$ (Fig. 10a). Transmission electron microscopy measurements revealed high dislocation density and numerous stacking faults, as would be expected considering the extensive plastic deformation involved in FS process (Fig. 10b). The colder temperatures achieved during FS avoided the formation of δ -ferrite, which contributed to an improved the corrosion resistance of the FS coatings compared to those obtained by manual metal arc welding.

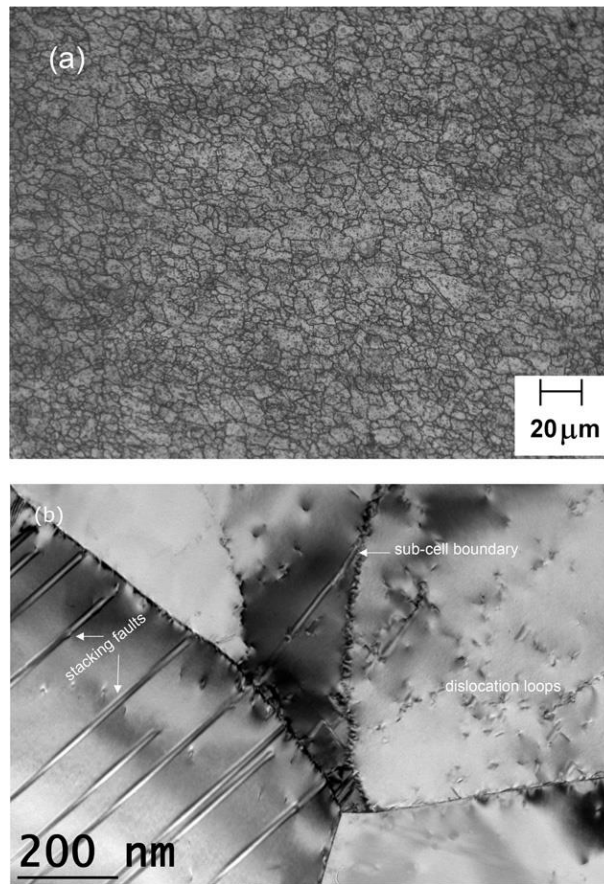


Fig. 10. Typical microstructures of AISI 316L coating. (a) Optical, (b) TEM (Puli and Janaki Ram, 2012a).

Gandra et al. (2012) addressed the deposition of mild steel over mild steel plates. The cooling rate enabled the growth of Widmanstatten ferrite within the coating and the transformation into a fine bainitic microstructure, as confirmed by hardness measurements around 300 HV, which were 115% higher compared to consumable rod.

2.1.2. Aluminium and magnesium alloys

In the deposition of aluminium alloys, the coating properties are determined mainly by the level of grain refinement and precipitate size and distribution, in case of a heat treatable alloy. Phase transformations are not observed as aluminium that already has a FCC crystalline structure. Vilaça et al. (2012) described the gradual transformations experienced by the AA6082-T6 aluminium rod during its deposition onto AA2024-T3

plates (Fig. 11). Consumable rod original microstructure is depicted in Fig. 11a, presenting an anisotropic grain structure aligned along the rod extrusion direction. Heat affected microstructures presenting some precipitate coarsening and grain growth can be seen in Fig. 11b, while evidences of in a compression/torsion plastic deformation are depicted in Fig. 11c and d.

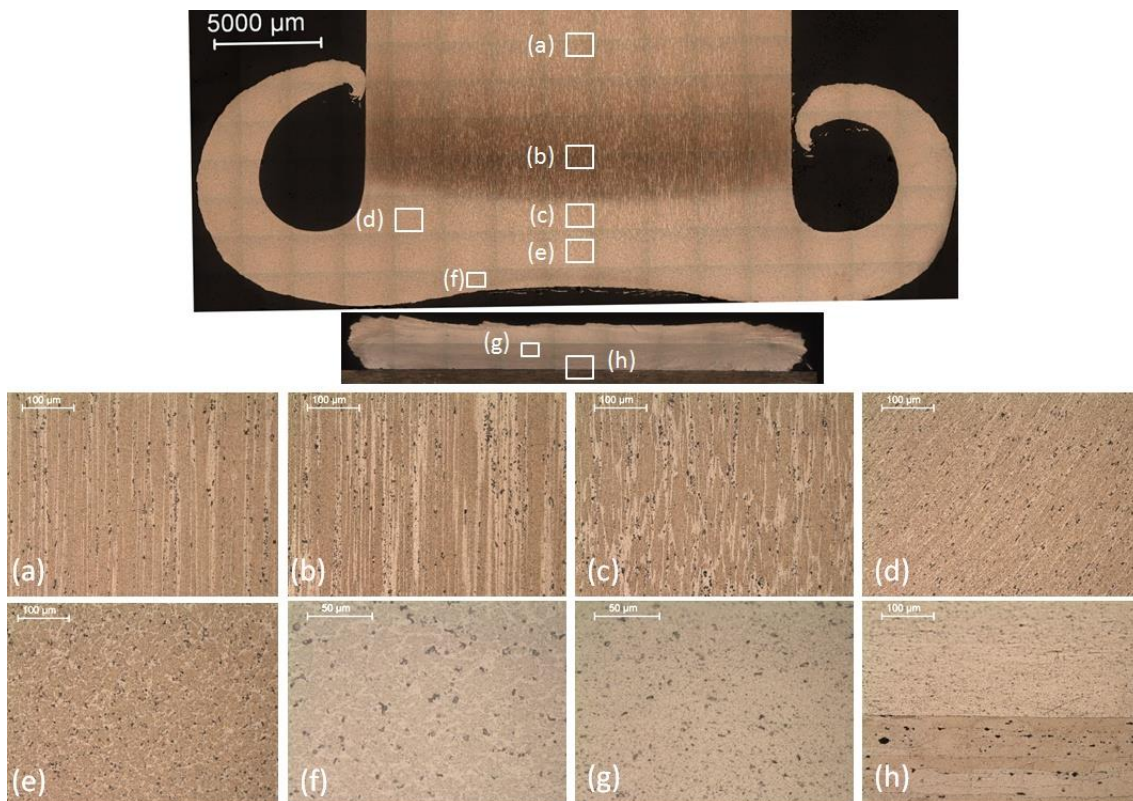


Fig. 11. Microstructural transformations during the FS of AA6082-T6 over AA2024-T3. (a) Consumable base material, (b) Heat affected zone, (c) Compression-driven TMAZ, (d) Torsion-driven TMAZ (e-f) Fully recrystallized microstructure, (g) Deposited material, (h) Bonding interface (Vilaça et al., 2012).

The combination of plastic deformation and heat generation leads to a dynamic recrystallization with the nucleation and growth of a new set of grains (Fig. 11e and f). Heat is lost mainly by conduction to the substrate, creating a 2.2 mm deep substrate HAZ. A fully bonded interface can be seen in Fig. 11h.

Suhuddin et al. (2012) also addressed the microstructural transformations on the FS of an AA6082-T6 aluminium alloy over AA2024-T3. To understand the recrystallization mechanisms involved, the authors quantified the microstructural evolution at the consumable rod, with special emphasis on the transition from the thermo-mechanically affected zone onto the fully recrystallized region. Electron backscatter diffraction evidenced that shearing deformation was the predominant drive for dynamic recrystallization. Results also suggest that both continuous and discontinuous recrystallization processes occur.

Further work on the FS of AA6082 coatings over AA2024 was presented by Gandra et al. (2013a). Grain size measurements revealed an average size of $4.2 \pm 1.8 \mu\text{m}$ (Fig. 12a), accounting for a 33% grain refinement compared to the rod in as-received condition. Based on the standard deviation of the grain size measurements it is also evident that the coating presented a more homogeneous grain structure. Coating hardness is slightly higher near the surface reaching a maximum of 91 HV0.2. Although the coating presents a finer microstructure, the loss of the T6 artificial ageing treatment due to heat exposure results in a 15% hardness decrease compared to the rod in as-received condition. The hardness profile also evidences a 2.2 mm deep substrate HAZ, marked by a 5% hardness decrease. Fig. 12b presents the bonding interface between the coating and the substrate.

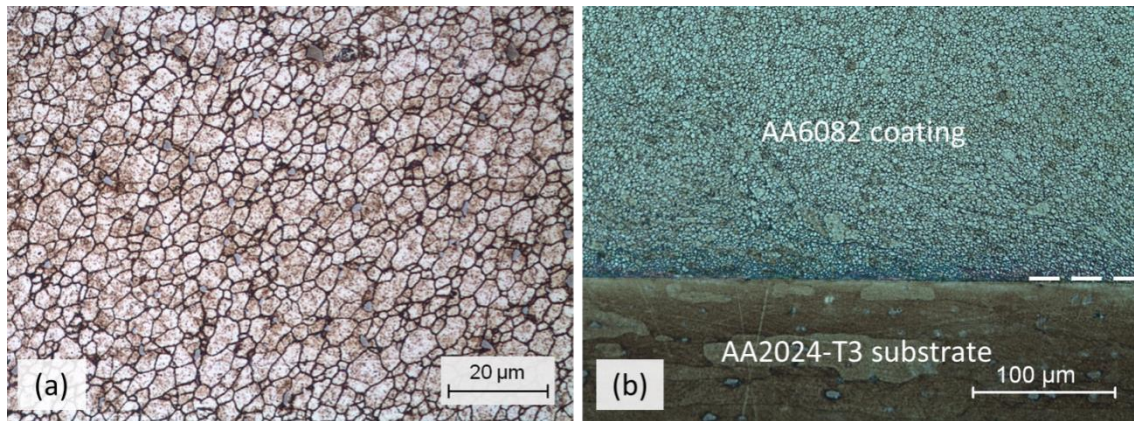


Fig. 12. Coating microstructure (a) and bonding interface (b) in the FS of AA6082-T6 over AA2024-T3 (Gandra et al., 2013b).

Sakihama et al. (2003) investigated the deposition of AA5052 PH-34 aluminium alloy over plates of the same material. Coating peak temperatures of about 527 °C were reported. The microstructure of the deposit was finer than that of the substrate and consumable rod. The coatings presented a mean hardness value of 57 HV, which is similar to the annealed condition of the aluminium alloy used. The HAZ of the substrate reached a 3 mm depth. Similar findings regarding the FS of aluminium alloys were presented by Tokisue et al. (2006).

Similar transformations are reported in the FS of magnesium alloys. Nakama et al. (2008b) used AZ91 casting bars as consumable rods to perform linear depositions over AZ31 magnesium plates. The deposits presented a finer and homogeneous grain structure compared to the consumable rod original condition and plate base material. Thermocouple measurements at the substrate suggest that the coating material reached a peak temperature of approximately 265 °C, resulting in the dynamic recrystallization of the AZ91 cast microstructure. As a result, there was an increase in hardness of approximately 40%, as compared to the wear resistance in the substrate. Fig. 13 shows the coating interface and base materials microstructure for several rotation speeds.

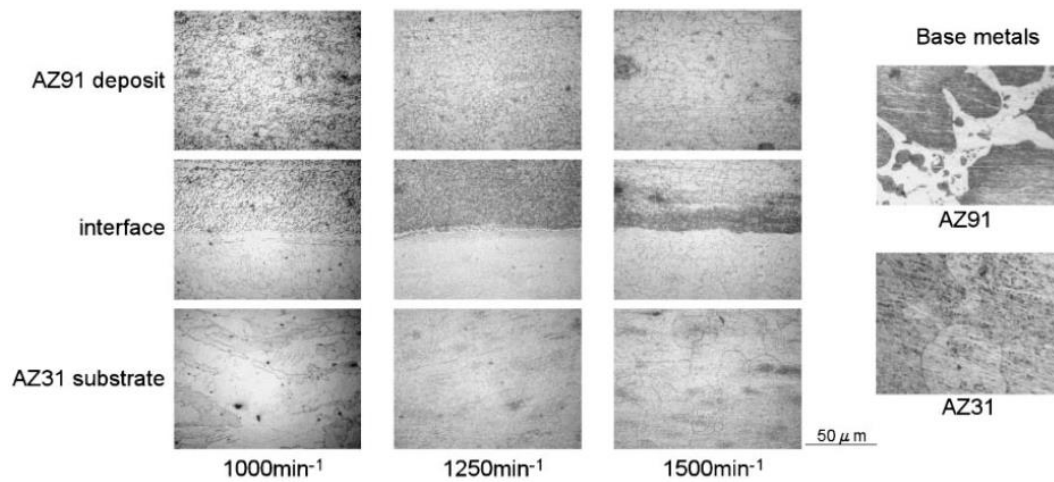


Fig. 13. Microstructural details in the FS of AZ91 over AZ31 (Nakama et al., 2008b).

2.1.3. Titanium alloys

Preliminary studies on the similar deposition of Titanium 6.4 alloy were reported by Beyer et al. (2003). As depicted by Fig. 14a, the deposited layer presented partly martensitic acicular α -phases, resulting in hardness values of about 400 HV 0.2.

Additionally, the bonding interface presented some defect, which contributed to a brittle fracture of the coating under push-off characterization (Fig. 14b).

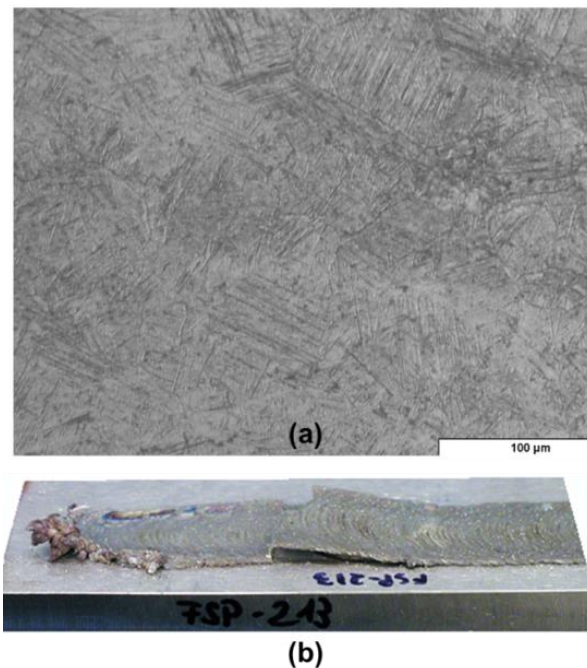


Fig. 14. FS of Titanium 6.4 consumable rod and plate. (a) Coating microstructure and (b) push-off characterization (Beyer et al., 2003).

2.1.4. NiAl Bronze

Hanke et al. (2011) investigated the cavitation erosion mechanisms of NiAl Bronze coating layers deposited by FS on plates of the same material. As shown in Fig. 15a, the coating presents a fine microstructure containing lamellar and globular α phases and quenched β phases, in contrast with the typical as-cast microstructure of the substrate (Fig. 15c). Closer to the surface of the layer, the α phase presents a more pronounced lamellar shape, changing to globular closer to the substrate (Fig. 15b). This is related to the faster cooling rate experienced at coating surface. The average wear rate of the coating material was half of that of the substrate, while the beginning of the wear process took twice as long (Fig. 15d). This was attributed mainly to the more ductile crack propagation within the coatings, in comparison with that developed throughout the coarse and anisotropic casting microstructure of the substrate.

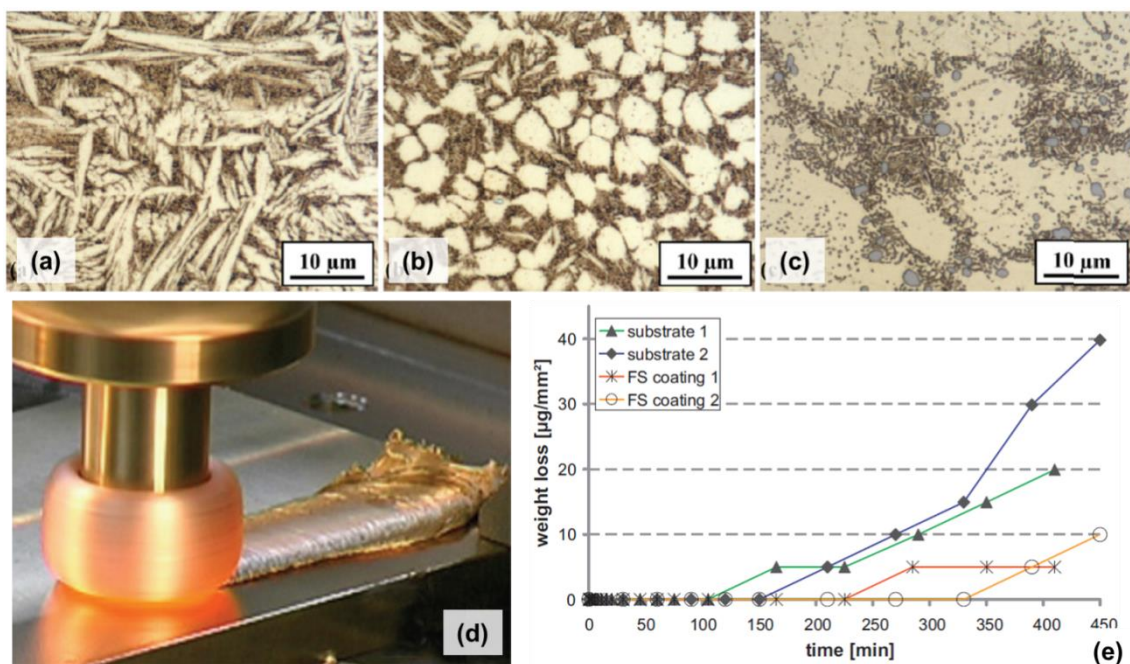


Fig. 15. Cavitation erosion study of NiAl-bronze layers generated by FS. (a) Microstructure of a friction surfaced sample. (b) coating close to surface, (c) coating close to substrate, (d) Coating production (Beyer et al., 2003), (e) Weight loss per worn area vs. cavitation test duration (Hanke et al., 2011).

2.2. Joining mechanisms

In friction-based processes, bonding can occur at the interface between (i) a material that is undergoing viscoplastic flow and (ii) surfaces which may be undergoing less severe deformation, as proposed by Thomas (2009a). The solid state joining mechanism is mostly controlled by diffusion, although the approximation to inter atomic equilibrium distances can also be found for lower temperature and higher pressure conditions at the joining interface.

In case of FS, the viscoplastic coating layer is pressed against the substrate at temperatures approximately 50 to 90% of the fusion temperature, enabling a diffusion bonding process, as was stated by Bedford et al. (2001). As reported by Shirzadi et al. (2001), plastic deformation can disrupt the relatively brittle oxide layers, establishing metal-to-metal contact and enabling the joining process along a thin interdiffusion layer. Batchelor et al. (1996) observed waved bonding interfaces between the deposit and the substrate, especially for dissimilar combinations in which the consumable rod material is tougher than the substrate or for higher axial forces. These waved interfaces also act as anchoring points, providing additional mechanical bonding.

The mixing of material along the interface layer was observed by Bedford and Richards (1985) measuring up to a 10 μm thickness in the deposition of high-speed steels over mild steel. Macedo (2011) stated that interfacial bonding is based on the mechanical interlocking between the waved surfaces and by a narrow diffusion layer, which was seen to measure approximately 6 μm , in the deposition of an AISI 310 stainless steel over AISI 1070.

In the deposition of AA6082-T6 aluminium alloy over AA2024-T3, Gandra et al. (2013a) estimated that diffusion occurred along a layer 8 μm thick. Sakihama et al.

(2003) addressed the tensile characterization of AA5052 PH-34 aluminium alloy depositions over plates of the same material.

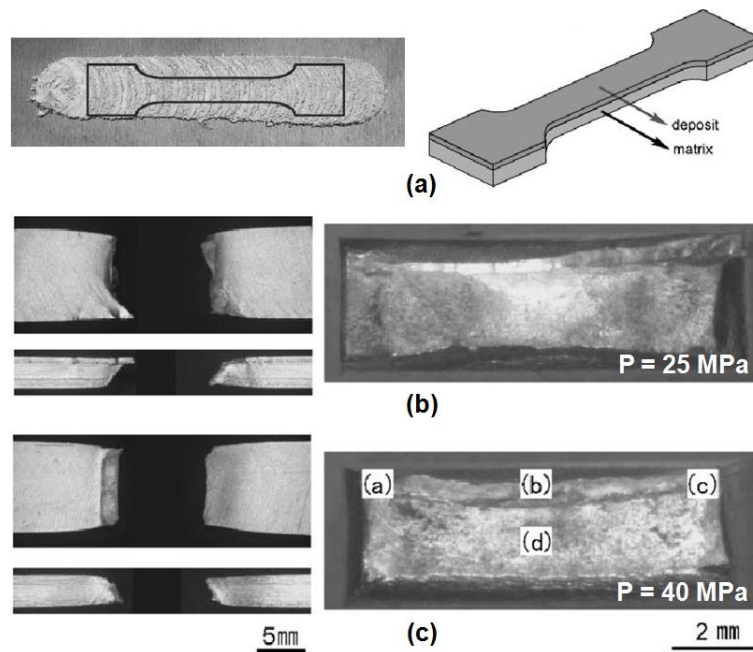


Fig. 16. Tensile testing of AA5052 PH-34 deposits. (a) Sample extraction. Macrofractographs of tensile tested specimens produced using contact pressures of (b) 25 MPa and (c) 40 MPa (Sakihama et al., 2003).

The tensile strength of the deposit was 11.2% lower than the base material, while elongation increased. Under tensile loading, flaking between the coating and the substrate was observed for the lower range of FS contact pressures (Fig. 16b). For contact pressures of 40 MPa, no flaking was observed and macrofractography evidenced a ductile fracture mechanism of both the coating and the substrate (Fig. 16a). Tokisue et al. (2006) addressed the deposition of AA2017 over AA5052. Bonding occurred by diffusion, although no evidences of material mixing were seen. Coated specimens presented tensile strengths as high as 267 MPa, showing a decrease in comparison with the rod original properties (414 MPa), while being higher than the substrate base material AA5052 plates (256 MPa).

Chandrasekaran et al. (1998) studied the interfacial joining process in the FS of several dissimilar material combinations (Fig. 17). Tool steel AISI 01 and Inconel 600 were successfully deposited over AISI 1020 mild steel. There were evidences of substrate plastic deformation, while frictional heat enabled the production of reaction products along the interface between the Inconel deposit and the mild steel substrate (Fig. 17b). No interfacial compounds were formed in the case of tool steel. Using consumable rods with a 12 mm diameter, it was also possible to deposit stainless steel AISI 304 and mild steel AISI 1020 of over AA5083 aluminium using a rotation speed of 3000 rpm and a 21.8 MPa contact pressure, as reported by Chandrasekaran et al. (1997).

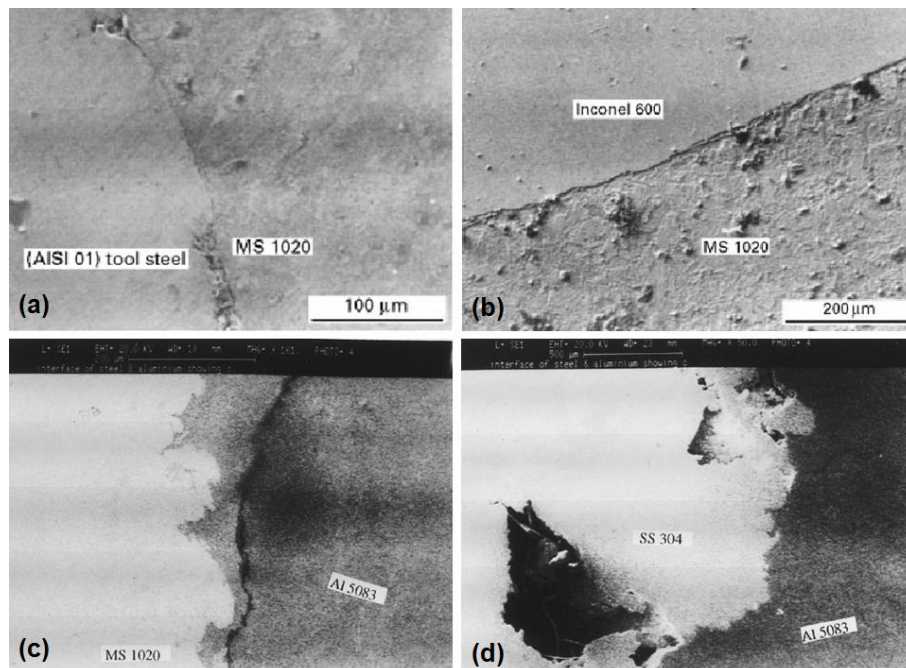


Fig. 17. Scanning electron micrograph of several material combinations produced by FS. (a) tool steel AISI 01 / mild steel AISI 1020, (b) Inconel 600 / mild steel AISI 1020, (c) mild steel AISI 1020, (d) Stainless steel AISI 304 / AA5083 aluminium alloy (Chandrasekaran et al., 1998; Chandrasekaran et al., 1997).

The mild steel deposits were bonded to the aluminium substrate mainly by mechanical locking and the observation of intermetallics at the interface suggests residual localized melting of the aluminium substrate (Fig. 17c). Although the SEM analysis revealed

cracks at the interface between the stainless steel deposit and the aluminium substrate, there were regions where no clear interfacial line was observed, suggesting a solid state bonding (Fig. 17d). No intermetallic phases for the stainless steel and aluminium combination were observed, possibly as these would require higher temperatures to occur. Deposition of aluminium over mild steel was achieved for high contact pressures, although the coatings presented poor adhesion and integrity. The FS of titanium rods onto mild steel has also been attempted, although no successful deposition was achieved.

Rao et al. (2012b) successfully deposited mild steel over copper and aluminium substrates. As depicted in Fig. 18a, the interface between the copper substrate and the steel layer present an intermixing region, resulting in a bonding shear strength of about 105 MPa. In the deposition of mild steel over aluminium alloy substrates, no evidences of diffusion bonding or material mixing was found at the interface. Samples presented an interfacial shear strength of around 112 MPa, most likely due to mechanical bonding, as seen in Fig. 18b. Similar results in the deposition of ferrous alloys over aluminium were presented by Chandrasekaran et al. (1997).

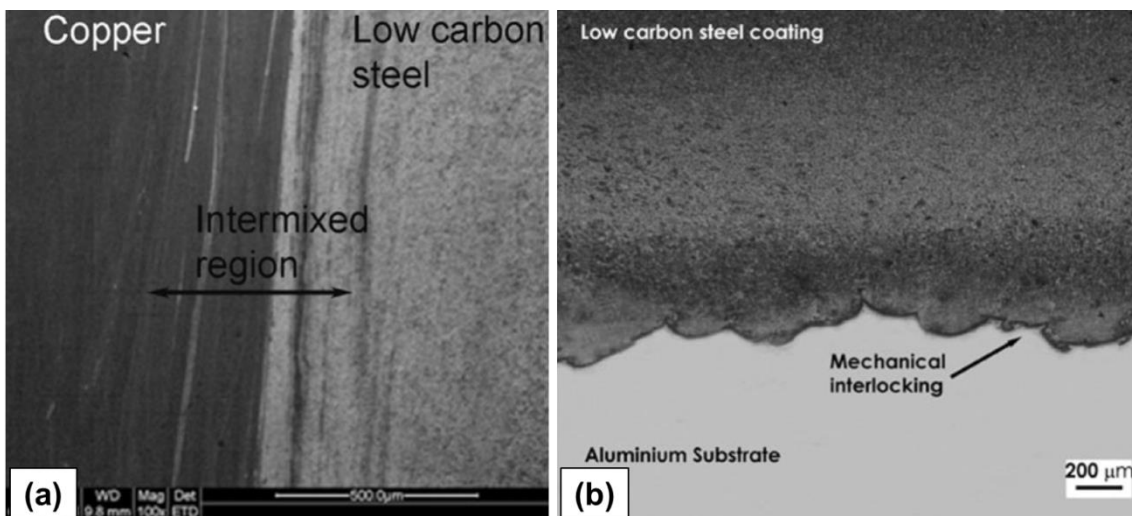


Fig. 18. Deposition of low carbon steel over (a) copper and (b) aluminium substrates (Rao et al., 2012b).

Batchelor et al. (1996) investigated the FS of several consumables, such as, AISI 304 stainless steel, AA6061 aluminium and brass on 5 mm thick mild-steel substrates.

Unlike stainless steel, which formed high strength deposits, the use of aluminium and brass consumables was not successful. The unsuccessful deposition of aluminium and brass over steel was attributed mainly due to their high thermal conductivity, which prevented the localized viscoplastic deformation of the rod tip. Similar effects were reported in the deposition of copper over aluminium AA2024, since the copper rods did not present any deformation. The heat conduction in copper is too high to allow for sufficient heat to concentrate at the tip of the rod in order to plasticise, as reported by Beyer et al. (2003).

Further results addressing the deposition of aluminium alloys over low carbon steel were recently presented by Sugandhi and Ravishankar (2012). Bonding was achieved using a 22 mm diameter AA1100 aluminium alloy rod, loaded with a 14 N/mm^2 contact pressure, rotating at 2500 rpm, while travelling at 16 mm/s. Rao et al. (2012b) explored the deposition of low carbon steel, copper, aluminium over titanium substrates, but no successful results were presented.

Regarding the application of FS to process magnesium alloys, Nakama et al. (2008b) addressed the deposition of AZ91 casting bars over AZ31 magnesium plates. Similar to aluminium, no mechanically mixed layer was observed at the weld interface between the deposit and the substrate. The use of magnesium substrates did not allow the deposition of steel, aluminium, titanium and copper, as attempted by Rao et al. (2012b).

Contact pressure and heat resulted in the plasticization of the magnesium substrate instead of the consumable rod tip.

Table 1 summarizes the materials deposited over steel substrates by FS. The investigations addressing the deposition over non-ferrous substrates are presented in Table 2.

Table 1. Reported FS material combinations deposited over steel substrates.

Consumable rods	Substrates	
	Carbon steel	Stainless steel
Mild steel	(Gandra et al., 2012)	
Alloy steel		
- AISI 4140	(Kramer de Macedo et al., 2010)	
- AISI 8620	(Kramer de Macedo et al., 2010)	
Austenitic stainless steel		
- AISI 304	(Govardhan et al., 2012; Rafi et al., 2011a)	
- AISI 310	(Kramer de Macedo et al., 2010; Rafi et al., 2010b)	
- AISI 316L	(Lambrineas and Jewsbury, 1992; Puli and Janaki Ram, 2012a)	
- AISI 321	(Lambrineas et al., 1990; Liu et al., 2009)	
Martensitic stainless steel		
- AISI 410	(Puli et al., 2011)	
- AISI 416	(Vitanov et al., 2001)	
- AISI 431	(Vitanov et al., 2001)	
- AISI 440	(Puli and Janaki Ram, 2012b)	(Katayama et al., 2009)
Tool steel		
- AISI O1	(Chandrasekaran et al., 1998; Chandrasekaran et al., 1997)	
- AISI D2	(Rao et al., 2012c)	
- AISI H13	(Rafi et al., 2010a, 2011c)	
High speed steels		
- BM2, BT15, ASP30	(Bedford et al., 2001)	
Co-Cr based alloys		
- Stellite 6,12	(Rao et al., 2012a)	(Bedford et al., 1995; Vitanov and Javaid, 2010)
Ni-Cr based alloys		
- Inconel 600	(Chandrasekaran et al., 1998; Chandrasekaran et al., 1997)	
Aluminium		
- AA1100	(Sugandhi and Ravishankar, 2012)	
- AA6061	(Batchelor et al., 1996)	
Titanium (Pure)	(Chandrasekaran et al., 1997)	
Brass	(Batchelor et al., 1996)	
Bronze	(Kershenbaum, 1972; Kershenbaum and Averbukh, 1964)	
Copper (pure)	(Rao et al., 2012c)	

 *not successful*

Table 2. Reported FS material depositions over non-ferrous substrates.

Consumable rod	Substrate					
	Aluminium	Magnesium	Copper	NiAl Bronze	Inconel	Titanium
Mild steel	(Chandrasekaran et al., 1997; Rao et al., 2012b)	(Rao et al., 2012b)	(Rao et al., 2012b)		(Rao et al., 2012b)	(Rao et al., 2012b)
Stainless steel (AISI 304)	(Chandrasekaran et al., 1997)					
Aluminium						
- AA1100	(Beyer et al., 2003)					
- AA2124						(Reddy et al., 2011)
- AA6063	(Rao et al., 2012b)	(Rao et al., 2012b)	(Rao et al., 2012b)		(Rao et al., 2012b)	(Rao et al., 2012b)
- AA6082	(Gandra et al., 2013a; Ravi, 2011; Suhuddin et al., 2012; Vilaça et al., 2012)					
- AA5052	(Sakihama et al., 2003; Tokisue et al., 2006)					
Titanium						
- Pure	(Rao et al., 2012b)	(Rao et al., 2012b)	(Rao et al., 2012b)		(Rao et al., 2012b)	(Rao et al., 2012b)
- Ti-6Al-4V						(Beyer et al., 2003; Nicholas, 1993)
NiAl Bronze				(Hanke et al., 2011)		
Copper (Pure)	(Rao et al., 2012b)	(Rao et al., 2012b)	(Rao et al., 2012c)		(Rao et al., 2012b)	(Rao et al., 2012b)
Magnesium (AZ91)		(Nakama et al., 2008b)				

not successful

3. Process parameters

Coatings are evaluated mainly based on thickness, width and bond strength which are closely related to process parameters. Factors such as substrate thickness, rod diameter and material properties define the thermo-mechanical system, having a direct impact on the outcome result.

3.1. Equipment and control

In practice, there are several approaches to actuate the consumable rod, depending on the type of equipment used. Apart from defining the rotation and travel speed, the consumable rod consumption and hot-working pressure are determined either by controlling (i) the force or pressure applied on the consumable or (ii) the rod axial feed rate.

Regarding the first approach, force/pressure control consists in keeping constant the axial load applied on the consumable rod during deposition. This requires computer numeric control machines equipped with dedicated instrumentation (Vitanov et al., 2010). Some authors adapted milling machines, by installing pneumatic or hydraulic rams underneath the backing plate, forcing the working piece against the rotating consumable rod with a constant pressure/force. [Alternatively, Hanke et al. \(2011\)](#) converted a friction stud welding rigid gantry machines with linear axis provided by a movable table. The travel speed can be provided by moving the rotating consumable rod along the work piece ([Kalken, 2001](#)), the opposite ([Chandrasekaran et al., 1998](#)), or a combination of both ([Kramer de Macedo et al., 2010](#)).

Instead of using load control, [Vitanov et al. \(2010\)](#) explored the use of conventional CNC machines to set the rod feed rate, defined as the velocity at which the consumable rod is pushed along its axial direction against the substrate. By this approach, the

applied force will be a consequence and not a controllable variable. This allows reducing the equipment cost, as less instrumentation is needed. [The use of conventional CNC milling machines was pointed by Vitanov et al. \(2010\) as a solution to increase the commercial viability of the FS process.](#)

Force control provides a direct control on the hot-working conditions, being more suitable in the development of new applications. As supported by the studies of Vitanov et al. (2000), it is known that the axial force and the rod feed rate are closely related, and in a steady state deposition they remain approximately constant. Load controlled machines are probably more suitable for FS process development, allowing to determine the force/pressure for a suitable bonding, as well as, the associated rod feed rate. Based on those preliminary studies, the industrial use of FS is more likely to rely on rod feed rate control, taking advantage of the more economical machine costs.

[According to Vitanov and Javaid \(2010\), FS can be divided into two main stages based on the evolution of torque, force and temperature.](#) The process starts with an initial deformation period, as the rotating rod is pressed against the substrate, without lateral movement. This initial stage can be interpreted as a pre-heating step, allowing the material softening by frictional heating. When a viscoplastic layer is developed, the consumable rod starts to travel, thereby starting the deposition phase. [Liu et al. \(2008\) stated that by the end of the initial deformation phase, the main heat source shifts from interfacial friction to plastic deformation. Both the initial and the deposition phase can be either force/pressure or rod feed rate controlled.](#)

[Vitanov et al. \(2010\) based their extensive optimization research studies on rod feed rate control and evidenced how the force measured remained constant during deposition \(Fig. 19\).](#)

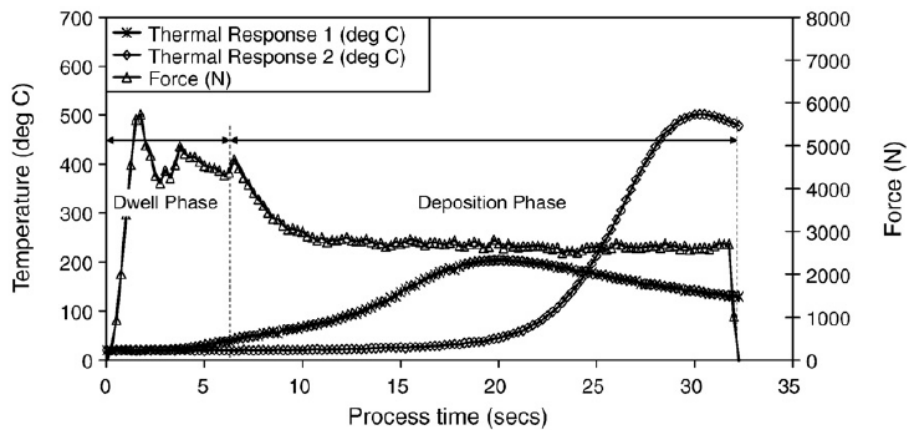


Fig. 19. Plot of axial force and thermocouple measurements performed at the substrate bottom surface. FS of Stellite 6 over AISI 316. Initial deformation and deposition phases were both rod feed rate controlled (Vitanov et al., 2010).

Gandra et al. (2011) related the evolution of process parameters with the metallurgical transformations and temperature cycle experienced in the deposition of mild steel. The authors used force control during deposition, while the initial deformation was determined by consumable rod feed rate control. Fig. 20 depicts the registered evolution of both the torque and applied force on the consumable rod, as well as, the displacement along the consumable rod axial direction. Infrared thermal imaging was used to measure the temperatures developed in the initial deformation region (AR01) and in a single point as the rod moved over it (SP01). The consumable rod had a 10 mm diameter. Five different process stages were observed. In the first stage, the machine develops the necessary torque to reach a consumable rotation speed of 2500 rpm, after which it starts to move downward along z towards the substrate. At the beginning of third stage, the rotating rod is pressed against the substrate with a constant downward speed of 1 mm/s (rod feed rate control). The initial plastic deformation of the rod tip results in a drastic increase in both temperature and force up to a maximum of 3.2 kN. For a consumed length of 1.2 mm, the temperature at the rod rubbing interface reaches about 1000 °C and a crown of incandescent plastic material is fully developed. As temperature softens

the rest of the consumable rod, both force and torque begin to drop, easing the on-going plunging to an approximately constant load of 2.3 kN and a temperature of 1020 °C. Torque begins to decrease gradually. For a 4 mm axial displacement, the consumable begins to travel over the substrate speeding to a velocity of 7.5 mm/s, starting the deposition phase. Rod vertical feed is now determined by the axial force control and the equipment applies a constant force of 5 kN. The FS process reaches a steady-state condition developing temperatures of about 1025 °C. The temperature range measured during initial plunge and deposition phases are consistent. This steady-state condition is also depicted by the approximately straight line displaying the axial displacement along the z axis. Notice that although the deposition was force controlled, the consumable rod axial displacement varied linear with time, meaning that the feed rate remained constant. After a 20 mm length rod consumption, the equipment automatically interrupted the process by extracting the rod.

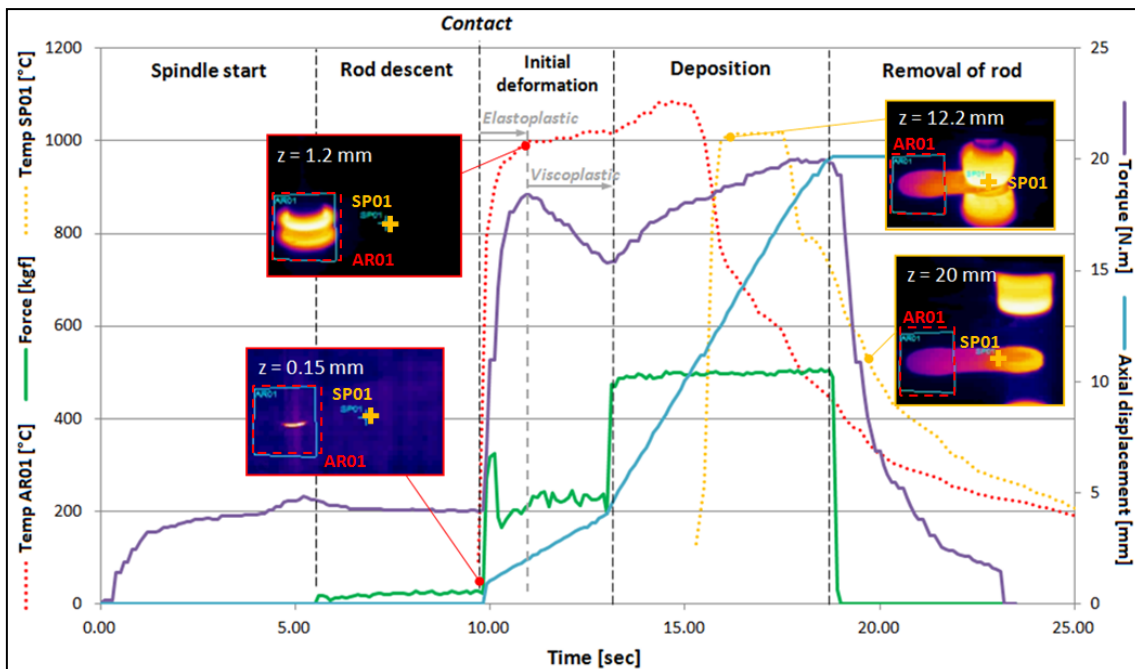


Fig. 20. Evolution of FS variables with time in the deposition of AISI 1020 over AISI 1020.

Initial deformation was controlled by consumable rod feed rate at 1 mm/s, using a 2500 rpm

rotation during a 4 mm length consumption. Deposition was force controlled using a 5 kN force and a 7.5 mm/s travel speed (Gandra et al., 2011).

As seen in Fig. 20, the initial deformation stage also features a transient stage of predominantly elastoplastic deformation, which ultimately evolves into a steady-state condition of viscoplastic deformation at temperatures around 1000 °C, marked by full austenization. Rafi et al. (2011c) and Bedford et al. (2001) also related the FS of steels to full austenization, as a condition required to perform FS. For aluminium alloys no phase transformation were reported, and the initial deformation stage is associated with the generation of the amount of heat and plastic deformation, required to induce a dynamic recrystallization, as reported by Tokisue et al. (2006). These transformations are responsible for the decrease of load and torque, as well as, the levelled evolution of temperature during the initial deformation stage. This phenomenon marks the achievement of the necessary starting conditions for FS, i.e., the extension of the plunge period will only result in extra flash formation under constant axial load, with no significant temperature development and no benefits for joining strength. Similar findings were also reported regarding the FS of stainless steels over mild steel by Rafi et al. (2011a), copper over copper by Rao et al. (2012c) and for aluminium alloys AA6082-T6 over AA2024-T3 by Gandra et al. (2013a). Rao et al. (2012c) proposed that the localized stress developed due to axial loading at the contact between consumable rod and substrate was equivalent to the flow stress of the plasticized material.

3.2. Influence of process parameters

In this process, heat is brought up by the combination of interfacial friction and viscoplastic deformation within the two contacting materials. However, the relative speed between the deposit and the substrate shears the bonding interface, disrupting and impairing the on-going diffusion bonding process. As such, it was found that both the

excessive rotation and travel speeds can be detrimental for joining, as the cross section bonded width decreases, as demonstrated by Shinoda et al. (1998). It could be expected that by increasing the rotation speed, the enhanced friction would produce more heat and always have a positive effect on bonding efficiency. However, some studies show that for lower rotations, the lower relative speed between the deposited material and the substrate can sometimes enable a more effective diffusion process and increase the contact area between the rod and the [deposit as shown by Kramer de Macedo et al. \(2010\)](#). Gandra et al. (2012) showed how tilting the consumable rod from 0 to 3° could result in an increase of bonded width. This can be justified by a more efficient confinement of viscoplastic material.

The effect of process parameters on the outcome result is complex and far from linear, being strongly dependent on the material combination used. However, there are some clear trends and effects which are continuously described in literature.

3.2.1. Axial force

[Shinoda et al. \(1998\)](#) investigated how the axial force resulted in an improvement of effectively bonded width, while leading to wider and thinner deposits. Excessive loads result in non-uniform deposition with a depression at the middle of the deposit. In contrast, insufficient axial forces result in poorly consolidated interfaces. This effect was reported by Gandra et al. (2012) in the deposition of mild steel over mild steel, as shown in Fig. 21.

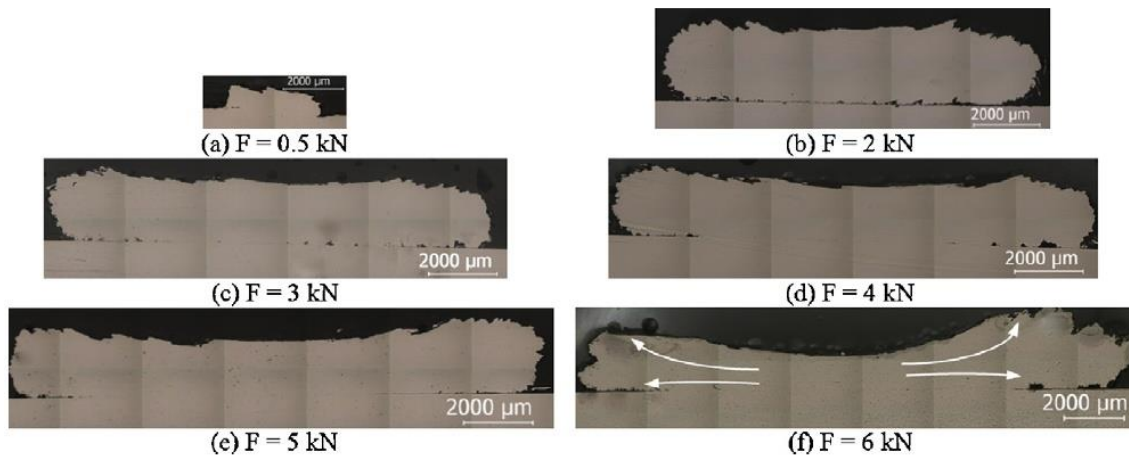


Fig. 21. Effect of axial force on coating cross section morphology and joining interface. FS of mild steel over mild steel. Consumable rods with a 10 mm diameter, using a 2500 rpm rotation speed and a 4.2 mm/s travel speed (Gandra et al., 2012).

Kalken (2001) observed that the increase of axial force can also lead to deeper substrate heat affected zones, as supported by Fig. 22, depicting the FS of stainless steel over mild steel.

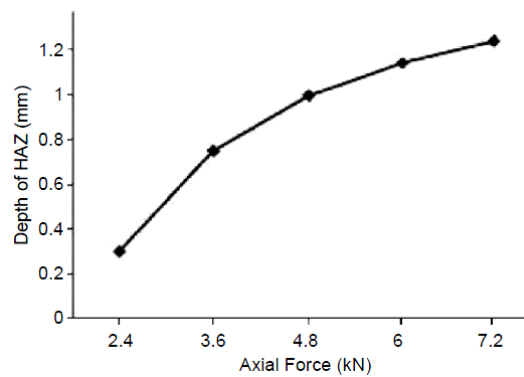


Fig. 22. Effect of axial force on substrate heat affected zone depth. FS of stainless steel over mild steel (Kalken, 2001).

Some studies also showed that the mechanical strength of the deposits is enhanced by the rise of axial force, as experienced by Sakihama et al. (2003) in the deposition of AA5052 aluminium alloy over plates of the same material.

3.2.2. Rotation speed

Rotation speed influences the bonding quality, coating width and roughness. Lower to intermediate rotation speeds enhance bonding quality, while excessive rotation speeds can also lead to a reduction of bonded width and substrate HAZ. Rafi et al. (2010a) observed that higher rotation speeds produce a more flat and regular deposit in the FS of H13 over mild steel (Fig. 23), with a more effective forging effect shaping the coating. Typically, the coating width decreases for higher rotation speeds.

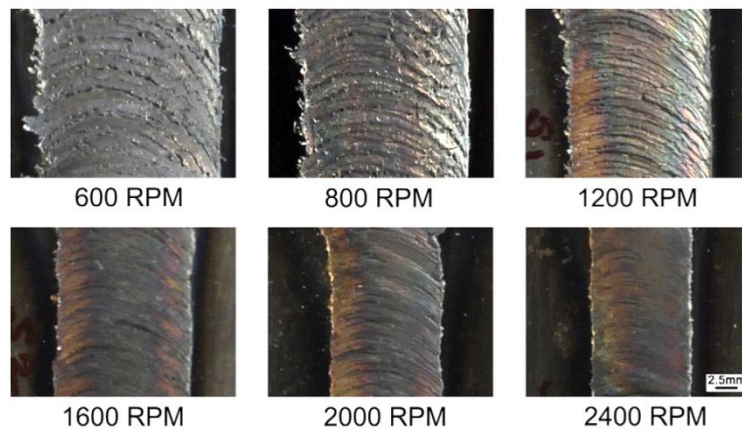


Fig. 23. Effect of rotation speed on coating surface roughness and width. FS of AISI H13 over mild steel. Consumable rod with a 18 mm diameter, force of 10 kN and a 4 mm/s travel speed (Rafi et al., 2010a).

Similar findings were reported in the FS of aluminium. In the deposition of AA5052 aluminium alloy over AA2017 plates, Tokisue et al. (2006) observed how the circular pattern in the coating surface was related with the rotation speed. The interval of circularity pattern became narrower for higher rotation speeds, thus resulting in a smoother surface finish. Sakihama et al. (2003) reported a reduction in both coating thickness and width for higher consumable rod rotation speeds in the FS of aluminium.

3.2.3. Travel speed

Travel speed strongly influences coating thickness and width, since it determines the rate at which material is deposited. As such, higher travel speeds result in a reduction in

both thickness and width, as was reported by Rafi et al. (2010b) in the FS of AISI 310 on mild steel (Fig. 24).

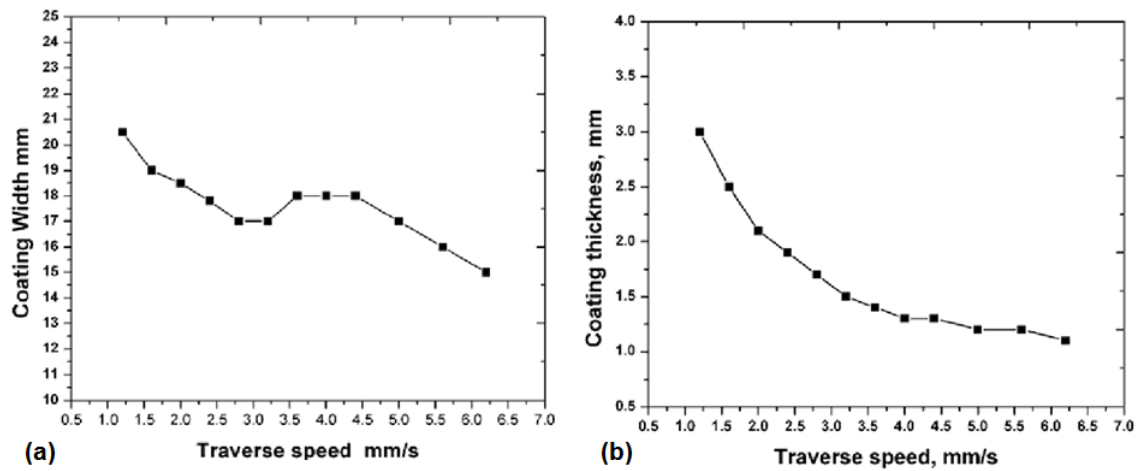


Fig. 24. Effect of travel speed on (a) width coating and (b) thickness. FS of austenitic stainless steel AISI 310 on low carbon Steel, using 18 mm diameter consumable rods, a 10 kN force and a rotation speed of 800 rpm (Rafi et al., 2010b).

The increase of travel speed, up to a certain extent, has also led to an increase on bonding strength, as observed by Rafi et al. (2010b) in the deposition of austenitic stainless steel AISI 310 (Fig. 25). Rafi et al. (2010a) reported two main failure mechanisms in the deposition of AISI H13 over mild steel, based on either the coating or the interface. Thicker coatings produced with lower travel speeds, were observed to fail at the interface at relatively lower shear loads. For higher travel speeds, failures were found to occur in the coating at higher shear loads. Bending tests also reflected this failure mode transition, as shown in Fig. 26. Faster travel speeds resulted in shorter heat exposure periods, resulting in less grain growth and limiting the substrate heat affection. Similar findings were also presented by Vitanov et al. (2000) in the FS of several grades of stainless steel and Gandra et al. (2012) in the deposition of mild steel.

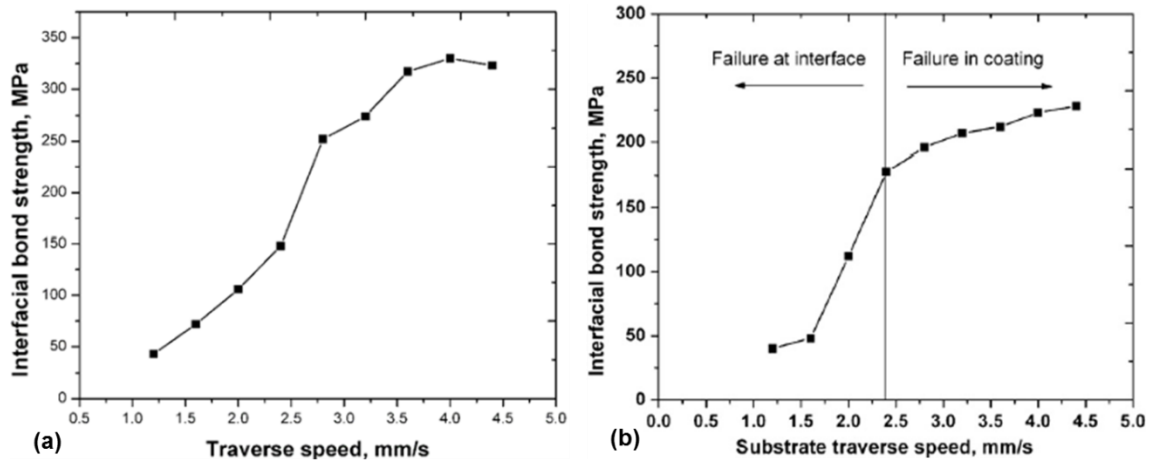


Fig. 25. Effect of travel speed on bonding shear strength in the deposition of (a) austenitic stainless steel AISI 310 (Rafi et al., 2010b), (b) hot work tool steel AISI H13 over mild steel substrates (Rafi et al., 2010a). Both investigations reported the use of 18 mm diameter consumable rods, a 10 kN force and a 800 rpm rotation speed.

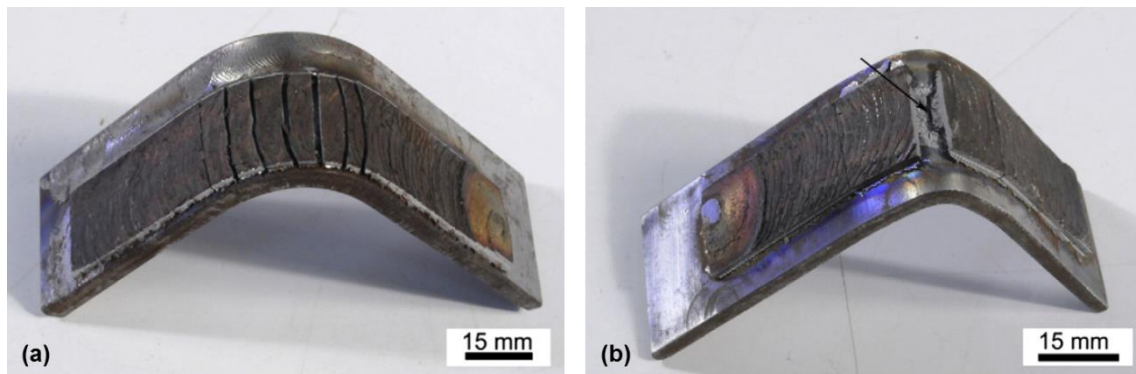


Fig. 26. Main bending failure modes reported in the deposition of AISI H13 over mild steel: (a) coating and (b) interface (Rafi et al., 2010a).

Thinner deposits also cool more rapidly yielding finer microstructures, as shown in Fig. 27 in the deposition of mild steel. However, bonding at coating edges usually deteriorates at excessive travel speeds, as shown by Vitanov et al. (2000).

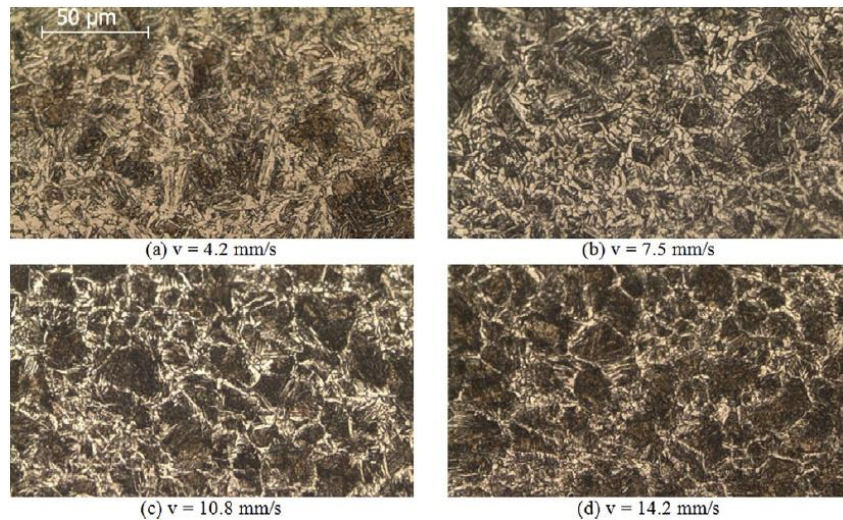


Fig. 27. Effect of travel speed on deposit bainic microstructure. Deposition of mild steel over mild steel using a 3 kN force, a 4.2 mm/s travel speed and a 10 mm diameter consumable rod (Gandra et al., 2012).

3.2.4. Consumable rod diameter

The influence of consumable rod diameter on coating heat exposure was first presented by Bedford et al. (2001). Empirically it was observed that the actual rubbing interface is not circular, but rather elliptical, as illustrated in Fig. 28a. The authors presented relationships between the exposure time, the rod diameter and travel speed (Fig. 28c). In the FS of steels, the diameter determined the time period extension in which the coating material undergoes austenitization before cooling. For instance, considering diameters from 10 to 32 mm and travel speeds of 1 mm/s, the region under the consumable rod will experience 10 to 32 seconds at maximum austenitization temperature (Fig. 28b and c). Regions at radial distances proportionally experience shorter periods of austenitization (Fig. 28b).

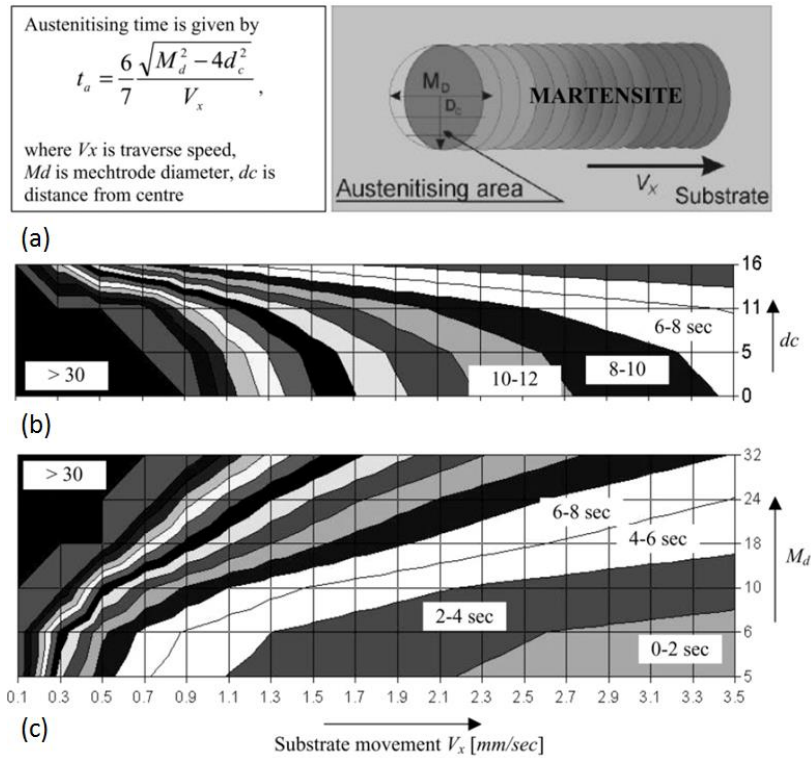


Fig. 28. Effect of consumable rod diameter and travel speed on austenitising kinetics. (a) Analytical relationship between the time spent in austenization domain, the traverse speed and the rod diameter, (b) effect of distance from centre (d_c) for a 32 mm diameter rod (here referred as mechtrode), (c) effect of rod diameter (M_d) (Bedford et al., 2001).

In conclusion, Fig. 29 summarizes the main process variables, parameters and control approaches, as well as, the main outputs of a given deposition. Examples of successful process parameter combinations are presented at Table 3.

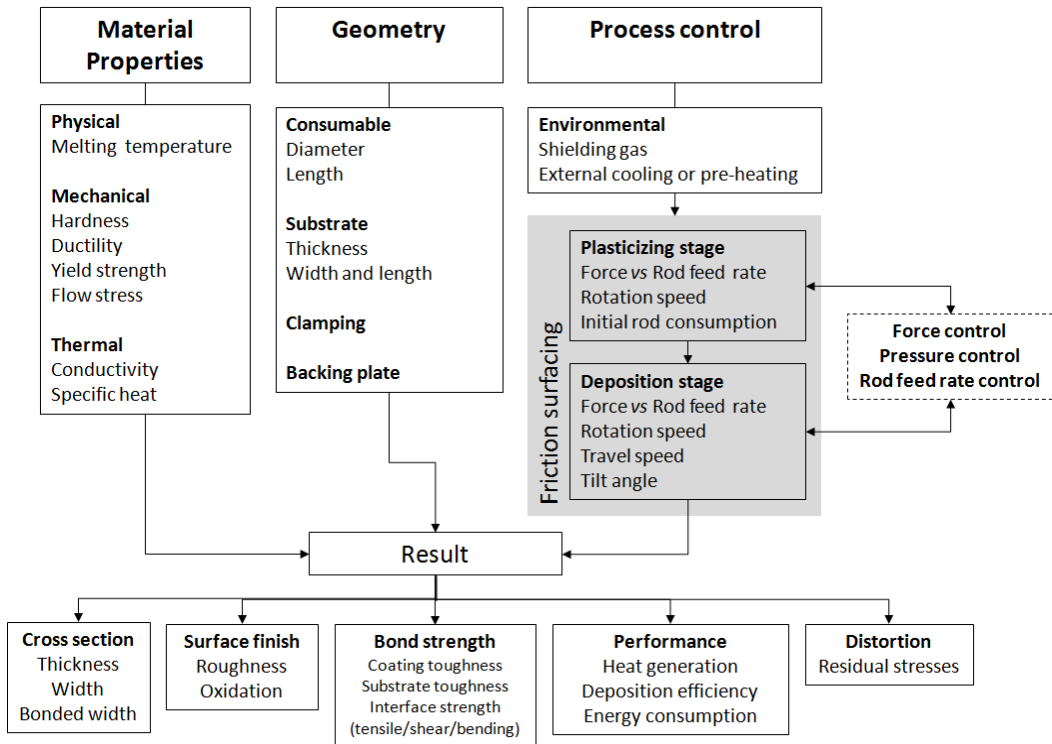


Fig. 29. FS process parameters and variables.

Table 3. Successful combinations of FS parameters.

Consumable rod		Substrate		Process parameters			Coating		Ref.
Material	Dia. [mm]	Material	Thick. [mm]	Force [kN]	Rotation speed [rpm]	Travel speed [mm/s]	Width [mm]	Thick. [mm]	
Mild steel	10	Mild steel	10	5	2500	7.5	15	1.8	(Gandra et al., 2012)
	20	AA6063	10	6	2000	2	n.a.	n.a.	(Rao et al., 2012b)
	20	Copper	10	8	2400	2	18	3	(Rao et al., 2012b)
	20	Inconel 800	10	10	1600	2	n.a.	n.a.	(Rao et al., 2012b)
Alloy steel									
- AISI 4140	20	AISI 1070	9	10.3	3500	8.5	15.35	0.78	(Kramer de Macedo et al., 2010)
- AISI 8620	20		9	10.3	3500	8.5	15.2	1.18	(Kramer de Macedo et al., 2010)
Stainless steel									
- AISI 304	15	Mild steel	12	8.3 *	2400	3.2	13.2	1.4	(Govardhan et al., 2012)
- AISI 310	18		8	10	800	4	18	1.5	(Rafi et al., 2010b)
- AISI 316	19		10	2.9	1400	8.2	12	1	(Lambrineas et al., 1990)
- AISI 321	19		10	4.4	1400	2.9	17	2.4	(Lambrineas et al., 1990)
- AISI 410	18		10	9.9 *	1200	3	19	1.8	(Puli et al., 2011)
- AISI 440	16		10	10 *	1150	3	14	1	(Puli and Janaki Ram, 2012b)
Tool Steel									
- AISI O1	12	Mild steel	n.a.	2.5 *	2500	2.9	n.a.	n.a.	(Chandrasekaran et al., 1997)
- AISI H13	18		8	10	800	4	18	1.3	(Rafi et al., 2010a)
Stellite 6	15	Mild steel	10	10	800	1.2	n.a.	n.a.	(Rao et al., 2012a)
Inconel 600	12	Mild steel	n.a.	2.5 *	3000	1.6	n.a.	n.a.	(Chandrasekaran et al., 1998)
Aluminium									
- AA1100	22	Mild steel	6	5.3 *	2500	16	20.22	0.89	(Sugandhi and Ravishankar, 2012)
- AA2017	20	AA5052	5	9.4 *	1200	9	21.3	1.1	(Tokisue et al., 2006)
- AA5052	20	AA5052	5	7.8 *	2000	9	19.6	3.8	(Sakihama et al., 2003)
- AA6082	20	AA2024	4.8	5	3000	7.5	20	2	(Gandra et al., 2013a)
Magnesium									
- AZ91	18	AZ31	6	10 *	1000	5	15	0.4	(Nakama et al., 2008b)
Titanium									
- Ti-6Al-4V	20	Ti-6Al-4V	10	0.22 *	4000	5	23	1.7	(Beyer et al., 2003)
NiAl Bronze									
- 81.60	20	80.90	10	15 *	4000	5	20	0.66	(Hanke et al., 2011)

(n.a.) information not available; (*) determined based on the applied pressure

4. Process modelling

Although most of the research work addressing FS is experimental, some complementary modelling approaches were presented to study and understand the material transfer process and heat generation. [As suggested by Jaworski et al. \(2000\), mathematical modelling can provide further understanding on the effect of process parameters on heat generation and the forces applied, especially at specific areas like the rubbing interface and the joining interface.](#) A validated model can calculate local strains, strains rates and stresses, which together with a temperature analysis, will allow to predict the microstructure evolution. The challenge is then to create a model able to fully describe the transient plunge period and stationary deposition period of the FS process. There are several concerns related to the modelling of FS, namely:

- FS process modelling does not allow geometric simplification by symmetry, because it deals with asymmetric material flow around the consumable rod.
- The materials thermo-mechanical properties vary throughout the process, depending on temperature and strain rate. These properties are not accessible for most of the engineering materials.
- During the deposition period the heat generated at the rubbing interface depends on an unknown varying friction coefficient.
- The heat energy flowing into the clamping system, substrate material and backing plate is fundamental in order to predict the metallurgical final properties and joining mechanisms.

Nonetheless several authors proposed some modelling alternatives. Liu et al. (2008) presented a physical model based on the theory of contact melting to study the material transferring mechanism in the deposition of AISI 321 stainless steel on mild steel. Based on thermocouple measurements performed along the axial direction of the

consumable rod, it was found that the temperature at the rubbing interface reaches a temperature just below the melting temperature, and as such, this region was interpreted considering a quasi-liquid layer concept, as shown in Fig. 30. The quasi-liquid layer is not interpreted as being in a fully liquid state. As proposed by Fukakusa (1996), it is treated as a liquid with special quality, composed by a viscous flowing material of special performance. The quasi-liquid layer forms on the real rotational contact plane and continuously transforms to solid during deposition. By observing the bottom surface of the consumable rods, the authors also reported that a slick concavity at the centre, which suggests that the energy concentrated in that region. Moreover, the bottom surface of the consumable rod presented no evidence of dry friction or adhesion, evidencing that friction occurred between the solid and viscous liquid, which supports the existence of the quasi-liquid layer.

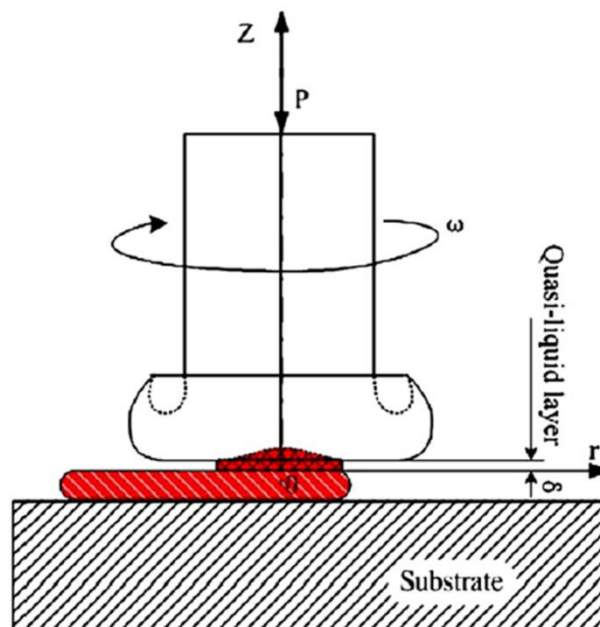


Fig. 30. Physical model of coating rod in friction surfacing based on the quasi-liquid layer concept (Liu et al., 2008).

Rafi et al. (2010a) also reported the formation of a concavity at the centre of the consumable rod, as shown in Fig. 31a. Although no microstructural evidence of fusion

was found in this region, the authors proposed that the concavity is based on vortex formation, as shown by the discernible spiral pattern at the end portion of the coatings (Fig. 31b), a well-known phenomenon in fluid mechanics.

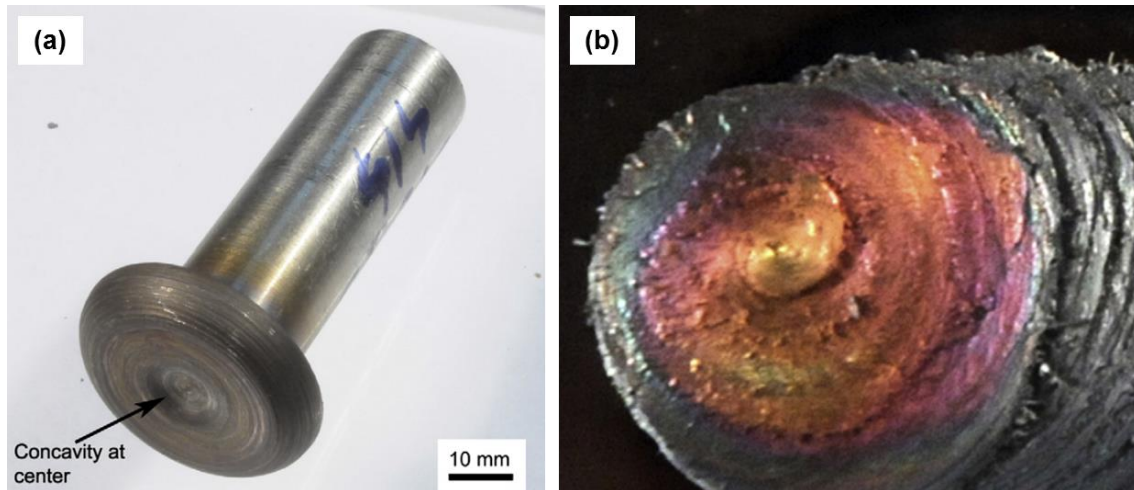


Fig. 31. Transferring process in the FS of AISI H13 over mild steel. (a) Condition of the consumable rod after friction surfacing, (b) end portion of a friction surfaced coating (Rafi et al., 2010a).

In subsequent investigations, Liu et al. (2009) used a finite difference method to model the thermal field developed at the consumable rod during the initial deformation stage. The authors defined an annulus element with a width of dr and an inner radius of r at the friction interface, as illustrated in Fig. 32.

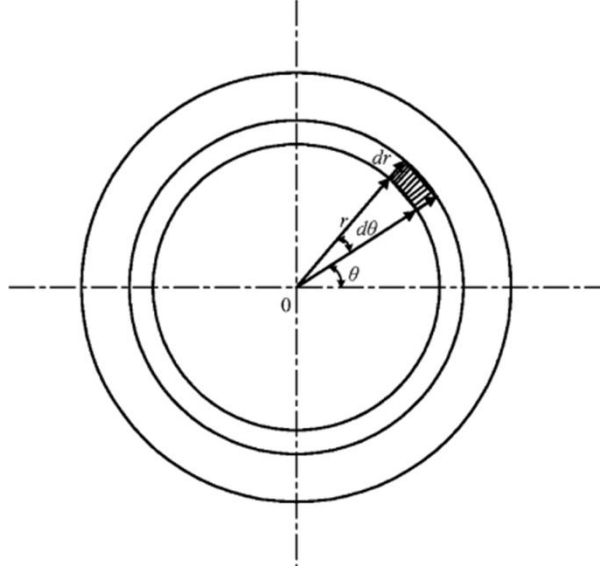


Fig. 32. Micro-element at friction interface (Liu et al., 2009).

Since the main heat source at the initial stage is produced mainly by normal and torsion friction at the annulus, the friction heating power (Q) at the interface was computed based on the approach proposed by Yao (2001), as given by Eq. (1).

$$Q = \int_0^R \frac{\mu n F}{20R^2} r \sqrt{1 - \left(\frac{r}{R}\right)^2} 2\pi r dr = \frac{\pi^2 R}{160} \mu n F \quad (1)$$

where, μ is the friction coefficient between the consumable rod and the substrate, R is the radius of the consumable rod, n is the rotation speed and F is the axial force.

Additionally, the heat stream density along at the annulus along the radial direction, $q(r)$, would be given by Eq. (2).

$$q(r) = \frac{\mu n F}{20R^2} r \sqrt{1 - \left(\frac{r}{R}\right)^2} \quad (2)$$

According to Zhang et al. (1997), the friction heat distributed to the consumable rod can be determined by Eq. (3).

$$q_c = \eta_1 q(r) \quad (3)$$

where,

$$\eta_1 = \frac{\sqrt{\lambda_1/\rho_1 c_1}}{\sqrt{\lambda_1/\rho_1 c_1} + \sqrt{\lambda_2/\rho_2 c_2}} \quad (4)$$

where, λ_1 and λ_2 are the thermal conductivity, ρ_1 and ρ_2 are the mass density and c_1 and c_2 are the specific heat capacity of the consumable rod and substrate, respectively. Using the present approach, the authors obtained an accurate correlation between the experimental measurements presenting a difference less than 10%, considering a consumable rod of AISI 321, as shown in Fig. 33. However, the present model can only be applied to the initial plasticizing stage, as it does not consider the travelling movement during deposition.

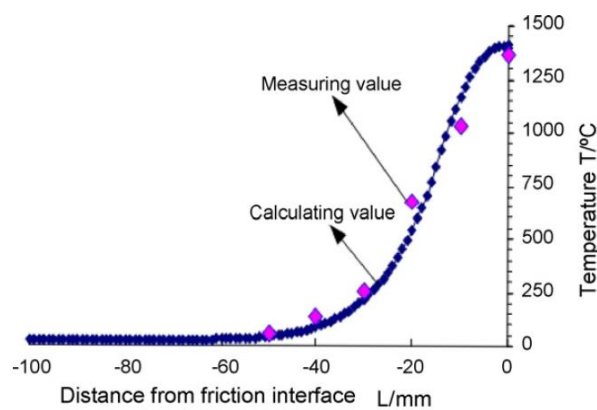


Fig. 33. Comparison between measured and calculated values of the thermal field generated along a initial plasticizing stage of 37 seconds, using a 4000 N, a 1825 rpm rotation speed (Liu et al., 2009).

Vitanov and Javaid (2010) modelled the thermal field during both the pre-heating and deposition stages using a finite element mode. A coupled transient thermal analysis was used to account both the initial plasticizing and deposition stage. This approach was validated by experimental thermocouple measurements at the substrate surface, presenting a co-relation with an 18% error, in the deposition of Stellite 6 and AISI 316. The authors also proposed that this model could be used to predict the temperature at the interface and subsequently, to elaborate on coating thickness, width and strength. Jaworski et al. (2000) also developed a finite element model that allowed to predict suitable travel speed values based on the thermal fields induced on more complex

substrate geometries, in the context of steam turbine blade repair. Mathematical simulations to estimate the FS parameters have also been proposed by Verevkin et al. (2003).

Significant research exists in the design of empirical-based models to successfully describe and optimize the process by speeding parameter selection. Vitanov et al. (2000) developed a decision support system to correlate the resulting bond strength, coating thickness and width with the most relevant process parameters (force, rotation and travel speeds). The optimization process was tested for the deposition of several grades of stainless steel (AISI 303, 304, 316, 416 and 431) over mild steel, using consumable diameters from 3 to 8 mm. The criteria for optimization was to extend the bonded width, while minimizing the undercut at the edges. Fig. 34 depicts some of the relationships achieved. Experimental data revealed that by increasing force, an increase in bond strength could be expected, while reducing coating thickness and the undercut. Traverse speed was found to be inversely proportional to the coating thickness. On the other hand, thicker or excessively thin coatings presented a weaker bonding strength. The undercut region was reduced by higher axial forces and increased for faster substrate movement. While the authors successfully modelled the effect on coating thickness and width, the bonding strength model failed to accurately describe the process behaviour.

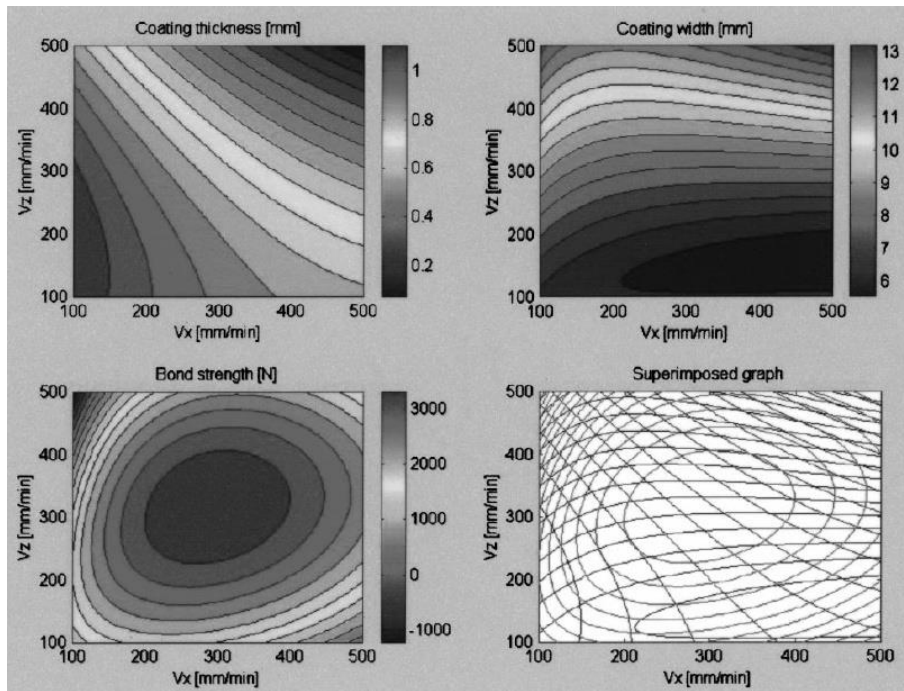


Fig. 34. Functional relationships between major process parameters and coating state variables in FS (Vitanov et al., 2000).

Later work done by Vitanov et al. (2001), combined artificial intelligence and modelling techniques, thereby developing a neurofuzzy decision support model. A real time process control was also addressed. By monitoring rod force, spindle speed, traverse speed, temperature and torque, the authors aimed to achieve the desirable coating thickness, width and bond strength. A process variable called bonding time was introduced to more effectively characterize the bonding process. Empirically, it can be observed that the actual bonding area is less than the original consumable rod diameter, as shown in Fig. 35a. To take this effect under account, bonding time was defined as the duration when the diameter of the heat generation area or bonding area passes entirely over a given point on the substrate. The authors estimated that the diameter of the bonding area is approximately 6/7 of the consumable diameter. Vitanov and Voutchkov (2005) reported that bonding time depends on travel speed and rod diameter, as shown in Fig. 35b. Lower travel speeds mean higher bonding times and, as a result, higher heat

inputs. Experimental data showed that faster traverse speeds, reduce bonding time, therefore increasing the coating undercut and reducing bond strength.

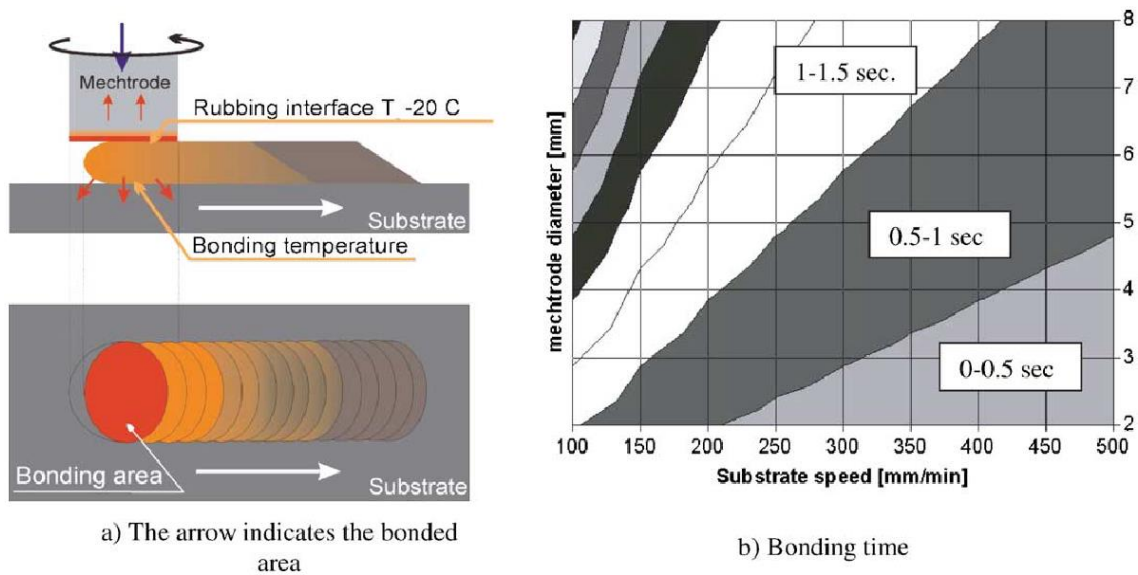


Fig. 35. FS bonding parameters. (a) bonding time definition, (b) influence of consumable rod diameter and travel speed on bonding time (Vitanov and Voutchkov, 2005).

Voutchkov et al. (2001) developed a process parameter optimization model combining both mathematical and statistical approaches. Procedures for the collection, storage and analysis of process information were also proposed. The authors based the first stage of process optimization on a visual assessment of the coating and the measurement of thickness and width. Using image-processing software, coating geometry and surface oxidation were also taken in consideration, as well as, the number of surface ripples. According to these authors, the different coloured oxidation patterns at the coating surface can be correlated with the deposition rate, oxidation and heat transfer, thus being an indicator of bonding efficiency. Based in this preliminary visual input, coatings were graded from 1 to 10, which enabled a selection for the following optimization stages. Fig. 36 depicts the effect of travel speed (V_x) and rod feed speed (V_z) on the coating appearance by visual characterization.

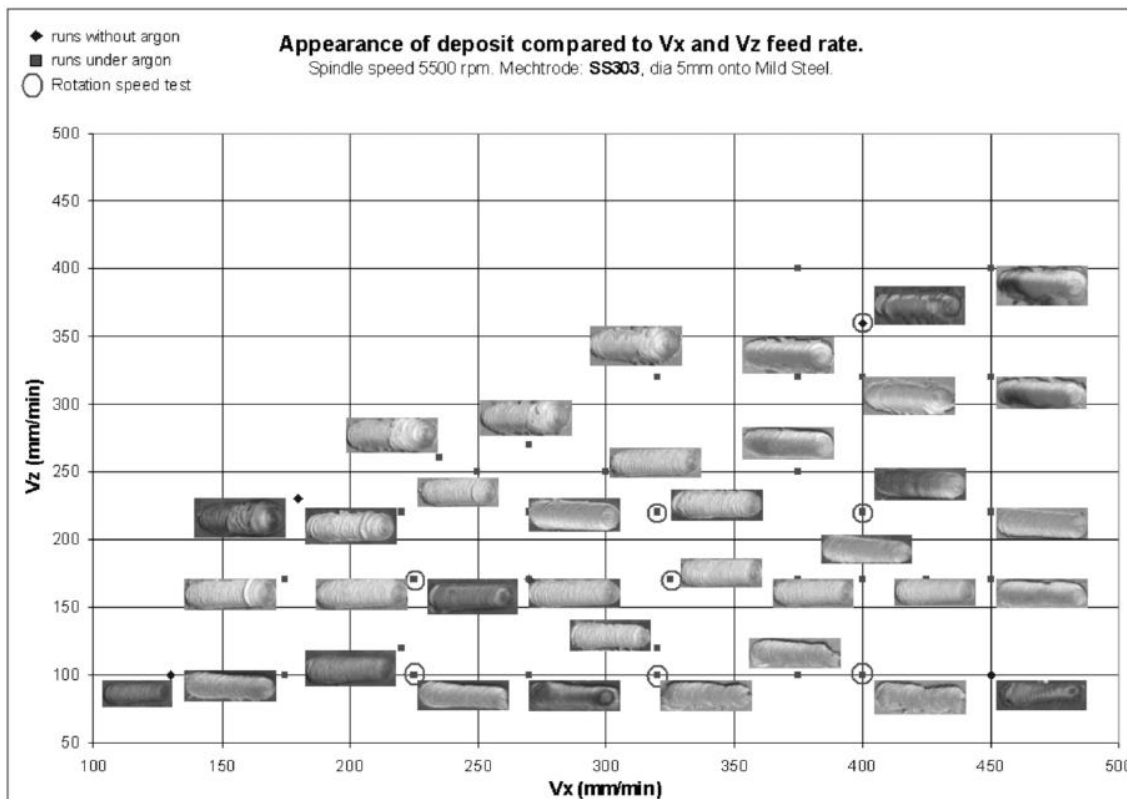


Fig. 36. Vx/Vz response surface - first stage of FS optimization (Voutchkov et al., 2001).

The second stage was based on the application of the Least Squares Method (LSM) to establish analytical relationships between process parameters and measurements, such as, thickness, width and bond strength. The final stage of the optimization, consisted on the use of a neural network model, which improved significantly the relationships obtained by the conventional regression model.

More recently, Vitanov et al. (2010) applied a response surface methodology (RSM) and statistical design of experiments techniques. Similar to previous works, the authors studied the effect of consumable rod feed rate, travel speed and rotation speed on process variables, such as: coating regularity, strength, average thickness. The normal force and the maximum temperature reached during deposition were also measured and considered as process responses. This methodology revealed that in the deposition of Stellite 6 over Stainless steel AISI 316, the ratio between consumable rod feed speed

and travel speed was one of the most significant factors in determining the coating quality and the normal load measured. It was also observed that higher ratios between the feed rate of the consumable and the travel speed resulted in superior bonding quality, as well as, lower to intermediate values of rotation speed. However, although some relationships between process variables were successfully presents, these were highly non-linear.

5. Configurations and designs

The process can be automated to perform non-linear depositions, providing good reproducibility (Vitanov et al., 2000). The absence of fusion and the fast cooling rates enables a great variety of positions and designs, as presented by Nicholas (1993) in Fig. 37. Circumferential applications were also presented by Katayama et al. (2009).

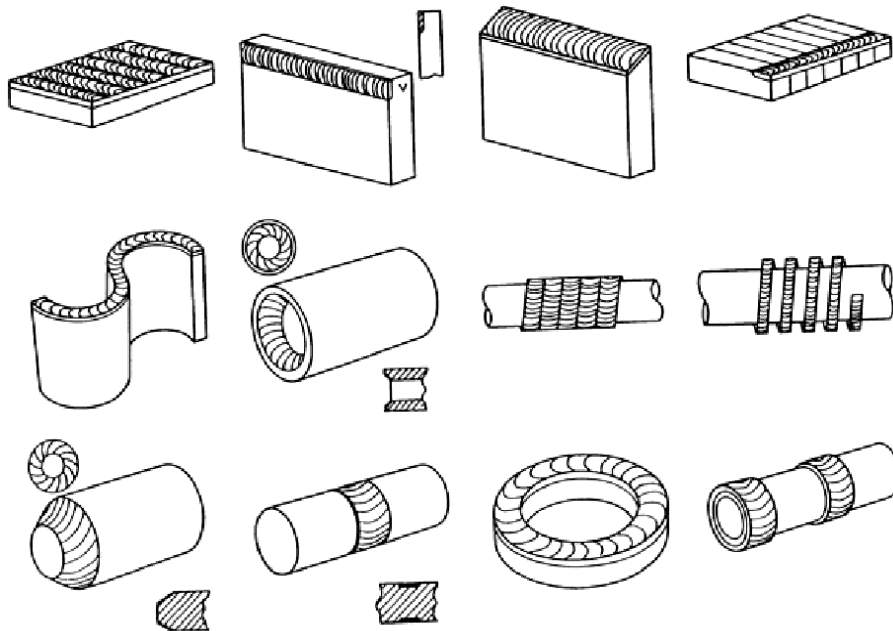


Fig. 37. Geometric arrangements for FS (Nicholas, 1993).

FS can be performed along complex trajectories. Some examples of FS path case studies can be seen in Fig. 38, depicting a single FS curvilinear path in both mild steel AISI 1020 and aluminium AA6082-T6.

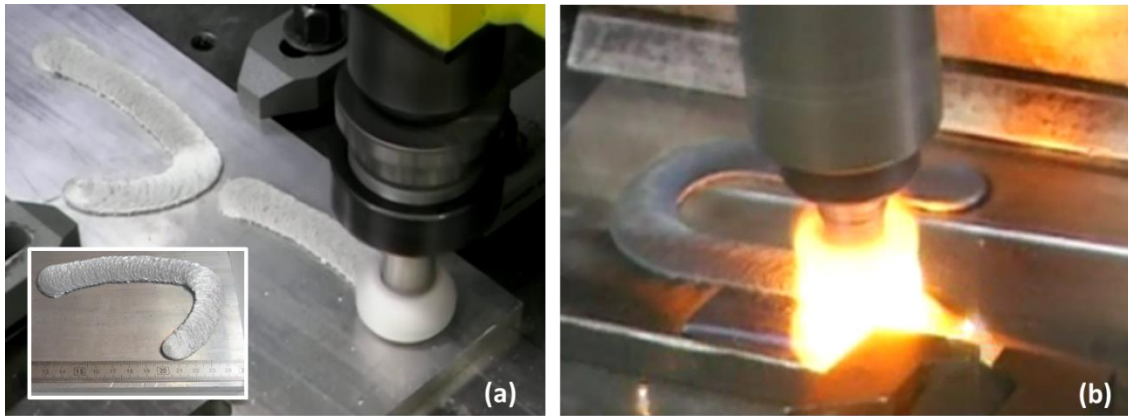


Fig. 38. Examples of non-linear trajectories of FS applied to (a) aluminium alloy AA6082 and (b) mild steel.

Area coverage using FS is performed by carrying several parallel depositions. Giving the weak bonding at the coating edges, the main issue in this approach is to prevent these defects from remaining inside the overall coating as the following layers are deposited. One way of dealing with this, is to assure that the undercut edge is overlapped by the following depositions, ensuring that the pressure and the heat are enough to consolidate the defect. Lambrineas and Jewsbury (1992) investigated different overlapping configurations in order to develop FS for area cladding for marine applications. Coatings of AISI 304 and 316 stainless steels were produced over mild steel. The overlapped depositions were not able to fully consolidate the unbonded edges of the deposits, leaving gaps at the interface between adjacent depositions. According to the authors, the failure to consolidate these defects limits the use of FS for areal coverage for applications requiring corrosion resistance.

Similar investigations addressing overlapping strategies were also performed by Tokisue et al. (2006) in the area coverage of AA2017 aluminium alloy over AA5052 aluminium alloy plates. As shown in Fig. 39, different overlapping ratios were tested, using offsets of 0, 5, 10 and 15 mm, either towards the advancing or the retreating side.

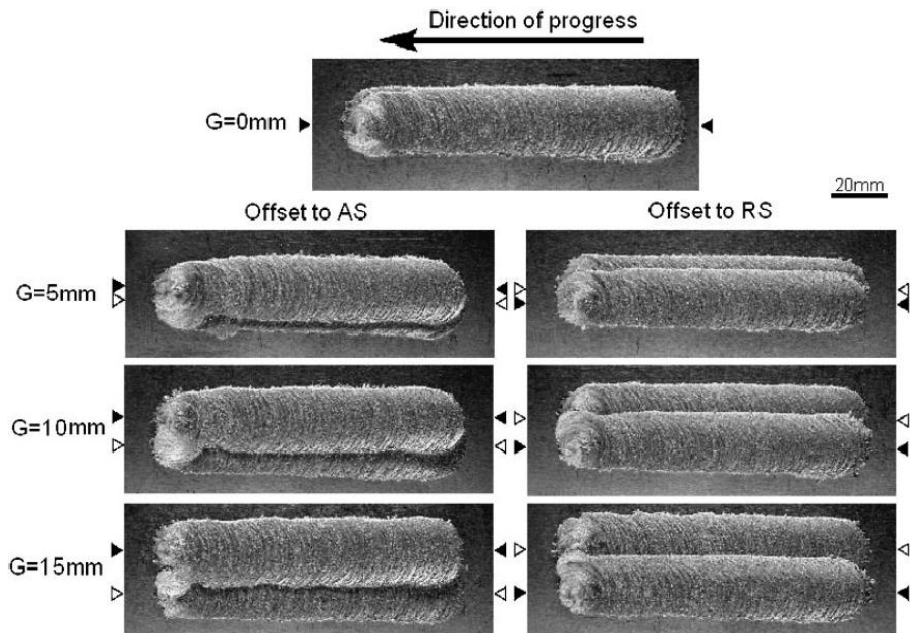


Fig. 39. Effect of overlapping distance on the appearance of multilayer deposits. FS of AA5052 over AA2017 (Tokisue et al., 2006).

Fig. 40 depicts the cross section macrographs of the multi-layer deposits. Overlapping by the second deposition enabled to consolidate the unbonded edge of the first deposit.

There was no clear interface between the first and second deposit and hardness profiles were relatively homogeneous (Fig. 41). The tensile strength of the multilayer reached around 300 MPa, being 12% higher than for the single depositions. Additionally, there was not a clear effect of overlapping offset on coating mechanical properties.



Fig. 40. Macrostructures of multilayer deposit for several overlapping distances. AA5052 over AA2017 (Tokisue et al., 2006).

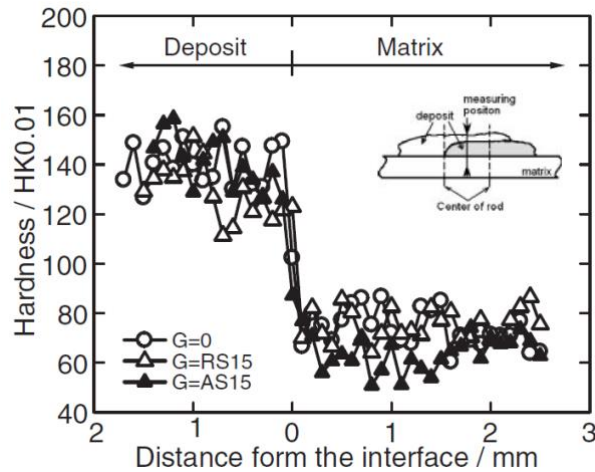


Fig. 41. Cross section hardness profile of multilayer deposits of AA5052 over AA2017 (Tokisue et al., 2006).

Despite the successful results presented by Tokisue et al. (2006) regarding the FS of aluminium, this overlapping approach has failed to consolidate the inter-layer defect when processing steel combinations. Considering the roll-over nature of the coating edges, the undercut surfaces are uneven and covered with oxide films, which interfere with surface bonding. Hence, Puli and Janaki Ram (2012b) has proposed to remove the unbonded edge by milling the coating in 3 mm, before further depositions. The consumable rod would then be placed, keeping a 0.3 mm gap between the rod and the machined edge of the previous layer. This 0.3 mm gap was determined to allow frictional contact between the edge of the previously deposited layer and the rotating consumable rod, without restraining its movement. The authors choose to machine the edge on the retreating side because this is the more irregular edge, as seen in previous sections. Using this overlapping procedure a sound bonding at the interface between adjacent coatings was achieved, in the FS of martensitic stainless steel AISI 440C over low carbon steel plates (Fig. 42a). As shown in Fig. 42b, multi-layer coatings were bending tested without showing any delamination or cracks. A similar approach was reported by Shinoda et al. (1998).

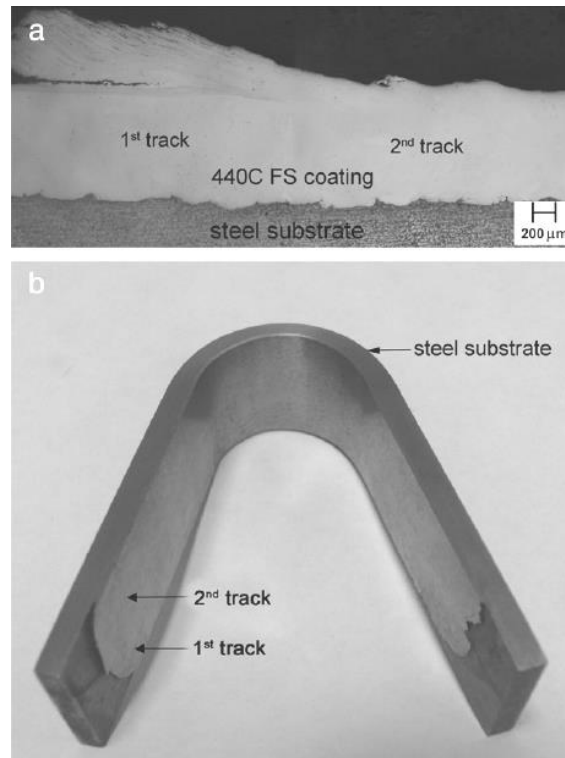


Fig. 42. (a) Cross-section of a multi-track friction surfaced coating of AISI 440C over low carbon steel. Displaying satisfactory bonding between successive tracks of deposited material. (b) Picture of a bent multi-track coated specimen (Puli and Janaki Ram, 2012b).

Another promising application consists on the vertical build-up of structures by performing successive fully overlapped depositions. Batchelor et al. (1996) studied the multi-layering using stainless steel consumables, performing up to three strongly-bonded depositions. It was possible to perform successive depositions directly over the as-deposited surface of the previous coating without any intermediate milling. Surface degreasing was found to be crucial for achieving sound depositions.

Fig. 43 depicts the manufacturing of a trapezoidal linear feature milled from the build-up of several AA6082-T6 friction surfaced passes, as proposed by Vilaça et al. (2012). FS allows the production of layered build-ups from which parts or component features can be manufactured.

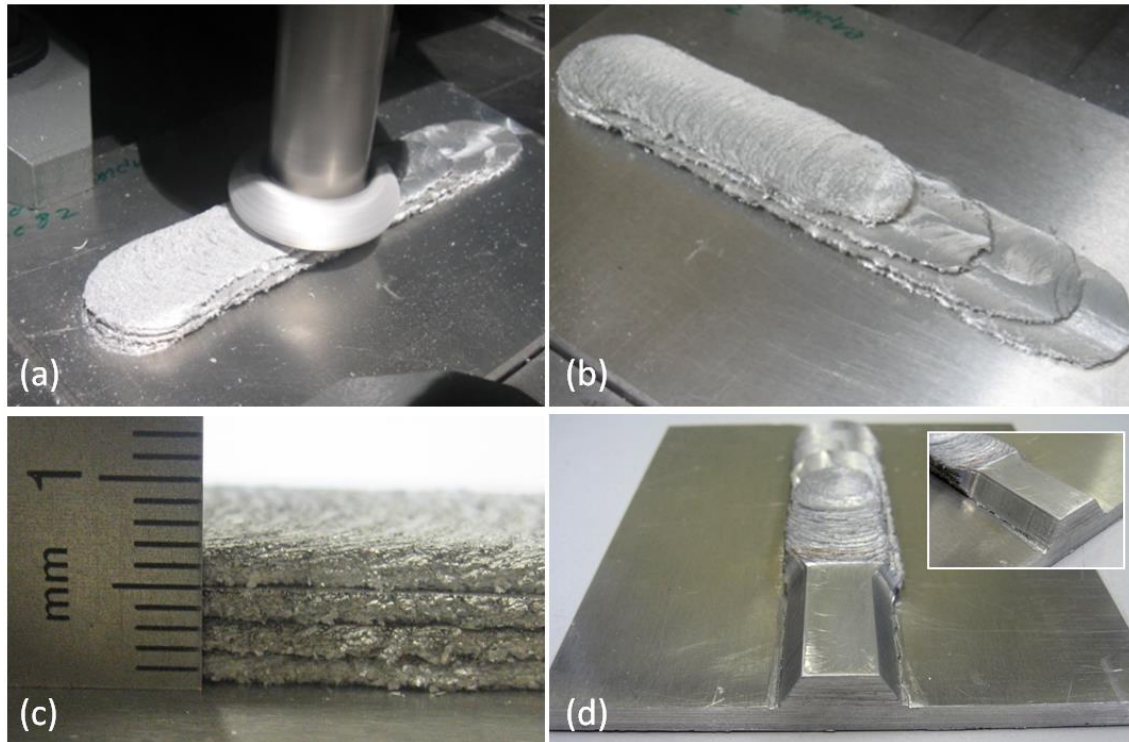


Fig. 43. Build-up by FS. (a) Successive deposition, (b) Bulk produced from four overlapped passes, (c) Detail of final thickness achieved, (d) Milling into final geometry (Vilaça et al., 2012).

Gandra et al. (2013b) addressed the production of multi-layer depositions of AA6082-T6, reporting that the heat flow from successive depositions resulted in the over-aging of the previous layers. This is evidenced by the hardness profile measured along the three layer deposition and the substrate, depicted in Fig. 44. Coating hardness decreases from the top to the bottom layer. The third and last deposition (L3) presents hardness values varying from 70 to 85 HV0.2, which are consistent with those of single layer depositions, as seen in previous work done by the same authors (Gandra et al., 2013a). Considering that no relevant grain size variations between layers were reported, it can be concluded that the hardness gradient along the multilayer coating is solely related to the coarsening of the second phase particles due to heat flow effect of subsequent deposits.

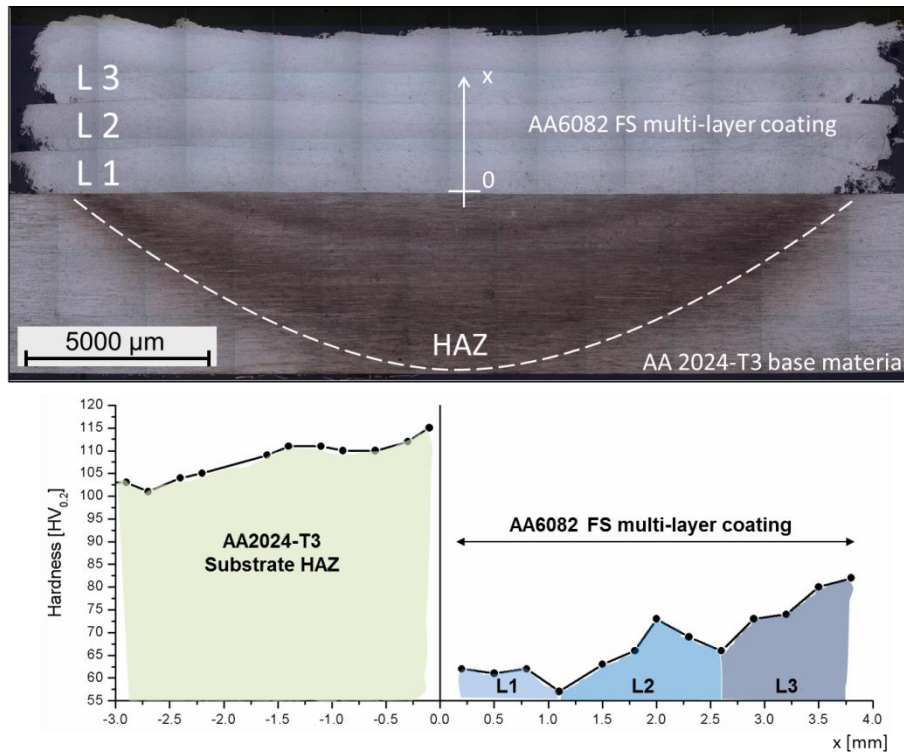


Fig. 44. Hardness profile for the non-reinforced multi-layer deposition sample. Base Material hardness (137 HV) and the rod (105 HV) (Gandra et al., 2013b).

Fig. 45 presents a continuous built-up process in contrast with the layer-by-layer built-up process.



Fig. 45. Continuous AA6082-T6 build-up by FS along a 3D helicoidally trajectory (Vilaça et al., 2012).

6. Technology developments

Several researchers proposed solutions to overcome the main disadvantages associated with the original FS concept. Industrial implementation impelled the development of preparation and post-processing techniques to suit the coatings according to application. Other authors addressed how pre-heating, cooling and gas protection could lead to improved results. The need to perform longer depositions led to the development of flash cutting devices and systems to support the consumable rod.

6.1. Consumable rod support systems

In FS the consumable rods used are essentially rigid, leading to the use of feed-forward mechanisms to apply the axial force or feed rate. Feed-forward mechanisms are limited in the length of consumable rod they can advance without interruption the feed. To prevent bucking, it is also more convenient to handle the consumables in short lengths. This compromises the ability to perform continuous depositions without interrupting the process for reloading. Since depositions are limited by the length of rod, this limits the length of deposition without compromising the coating integrity. Hanlon et al. (2010) and Pratt (1995), presented equipment solutions for supporting and continuous feeding of the consumable rod, while avoiding buckling. However, there is still a demand for systems capable of feeding a series of rods continuously without interrupting the application of pressure at the rubbing interface, as this is a potential research topic.

6.2. Pre-heating or cooling concepts

Whenever processing materials with a high melting temperature or thermal conductivity, pre-heating can be useful to soften and achieve the desired rate of plastic deformation. Pre-heating or cooling of either the substrate or the consumable can be a

solution to attenuate material thermal properties dissimilarities, like in the FS of aluminium over steel. Thicker substrates may also require pre-heating as their greater heat-sinking capability can impair the bonding process. In opposition, thinner substrates may require the use of thermal conductive backing plates to provide additional heat sinking.

There are known advantages related to the use of cooling to tailor the microstructural transformations following dynamic recrystallization. In solid state processes, such as, friction stir welding and processing, the induction of faster cooling rates has proven to prevent an extensive growth of the recrystallized grain structure and the control of precipitation hardening, as proposed by Mishra and Ma (2005).

One of the first references on the application of cooling systems to FS was described in the patent by Bedford (1991). The patent addresses the benefits of cooling the substrate, in the production of spot depositions by a so called “touchdown” technique (Nicholas, 1993). Since there is no travel movement, a circular deposit is produced, which increases in thickness until the extraction of the consumable rod. According to the inventors, the heat extraction along the substrate will enable to cool and consolidate the deposited material, pushing the viscoplastic rubbing interface way from the substrate surface, along the consumable rod axis. This allows a controlled development of both the deposited thickness and microstructural features.

To study the effect of the surrounding environment, Li and Shinoda (2000) deposited a martensitic stainless steel (AISI 440C) on a low carbon steel substrate in both air and underwater environments. Comparing to the depositions performed in air, underwater FS was found to result in improved deposition efficiency, finer coating microstructures and higher hardness. Underwater FS was also investigated by Beyer et al. (2003) in the

deposition of stainless steel on mild steel, as well as, of Inconel on X65 steel (Fig. 46a). Results showed that the flash development decreased and the initial plasticizing time period was extended in comparison with performing deposition in a dry environment. Underwater cooling enabled to produce longer depositions for the same consumable rod consumption.

Since the use of a water bath is limited to horizontal applications, water spray cooling was developed by Ravi (2011) and Suhuddin et al. (2012), thereby combining the advantages of underwater cooling with higher process flexibility.

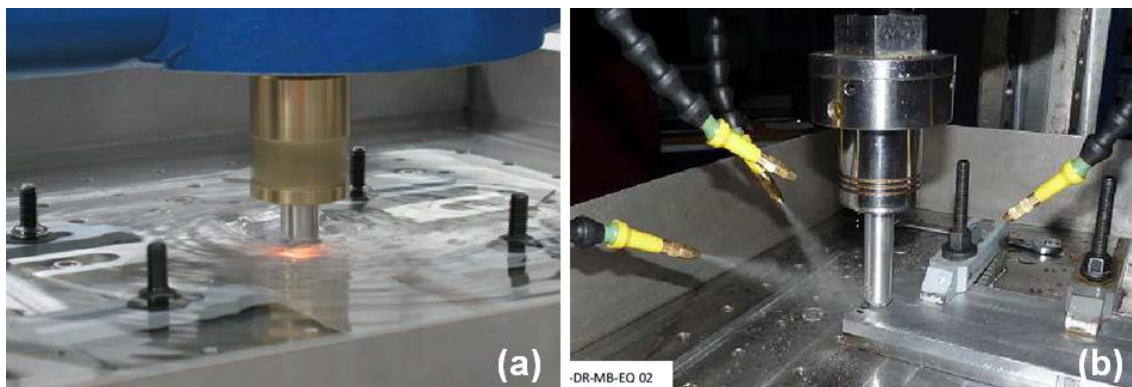


Fig. 46. Water based cooling in FS. (a) Underwater FS process in the deposition of stainless steel over mild steel (Beyer et al., 2003) and (b) Use of water spray cooling in the FS of AA6082 over AA2024 (Ravi, 2011).

Nozzles can be installed to cool both the flash and the newly deposited material (Fig. 46b). Krohn (2010) reported that a water flow up to 2 l/h was used in the FS of aluminium alloys. This water flow was sprayed by compressed air through five nozzles, forming fine droplets.

Cooling the flash enables to increase its toughness and consequently, the pressure distribution at the rubbing interface. Hence, forging closure is enhanced and pressure at the coating edges is increased, which results in wider bonded width and higher joining efficiencies. However, water spray cooling the newly deposited material, did not result

in a significant grain refinement or relevant increases of hardness or wear resistance. Cooling using liquid nitrogen can provide more promising results in terms of grain refinement, considering similar investigations in Friction Stir Processing (Ma, 2008).

6.3. Shielding gas

The FS process involves the generation of new surfaces which are highly reactive thus being prompt to oxidation in an open-air atmosphere. [Jenkins and Doyle \(1987\)](#) proposed that the use of an inert gas atmosphere was found to improve the performance of FS, since it limits the formation of oxide films at the interface.

[Batchelor et al. \(1996\)](#) reported the use of nitrogen for atmosphere protection, provided by a single jet directed to the rotating consumable rod. Although this arrangement did not successfully prevent oxidation, some basic protection was achieved. In succeeding investigations, [Chandrasekaran et al. \(1998\)](#) used a Perspex box chamber to fully confine the deposition area and ensure an inert atmosphere provided by argon. The use of argon has also been reported by [Voutchkov et al. \(2001\)](#). Additional environments were explored by [Jenkins and Doyle \(1989\)](#), namely partial vacuum and steam.

6.4. Flash cutting concepts

When coating larger lengths, the on-going flash formation will lead to excessive consumable rod upsets which can alter the pressure distribution at the rubbing interface and induce a transient deposition. These depositions result in the variation of coating properties, such as, width and/or thickness along the length, being due mainly to the variation of pressure and temperature conditions at the plasticized layer. Flash cutters can be used in order to prevent excessive flash growth, assuring a stationary process evolution in longer distance depositions, as proposed by [Beyer et al. \(2003\)](#).

6.5. Preparation and post-processing

Since FS is based on diffusion bonding mechanisms, surface cleaning and degreasing is crucial to achieve sound depositions.

The geometry of the rod tip has a significant effect on the beginning of plastic deformation. The use of chamfered consumable rods has been described by Beyer et al. (2003) as a way to increase the initial contact stress, while reducing the torque required for initial plasticizing.

For applications in which the consumable rod material has a highly superior mechanical strength than the substrate, it is common to perform the initial deformation stage on a starter plate, placed next to the substrate. Starter plates have a higher hardness than the substrate and are used just to initiate the plastic deformation. The consumable rod travels onto these substrate and perform the main deposition. It is also common to continue the deposition beyond the substrate into a finishing plate for rod extraction. These sacrificial plates are removed subsequent to deposition. Chandrasekaran et al. (1997) used mild steel starter plates to enable the rod initial plasticization, allowing the deposition of stainless steel and mild steel over the softer aluminium substrate. Further developments were presented by Rao et al. (2012b) in the deposition of mild steel over aluminium, by using the starter plate concept. As shown in Fig. 47, the consumables first contacted a mild steel starting plate and when the flash upset of viscoplastic material was produced, the deposition advanced onto the adjacent aluminium plate.

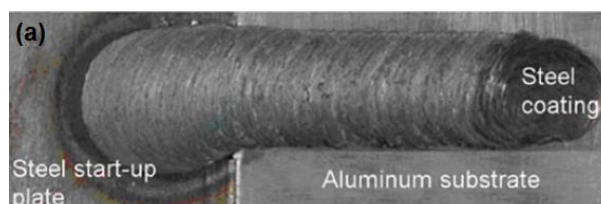


Fig. 47. Deposition of low carbon steel friction over aluminium substrate using a start-up plate (Rao et al., 2012b).

Since the coating surface is typically characterized by fine ripples, finishing post-processing is frequently required to even the surface. Some authors such as Vitanov et al. (2000) suggest that a removal of around 0.1 mm deep provides adequate surface finish for most applications.

Bedford and Richards (1990) described the deposition inside pre-machined slots, or channels, at the substrates. These openings are filled by FS, as they are designed to embed the deposited material within the substrate. Post-processing based on material removal is then used to shape the deposit into the desirable geometry, depending on part specifications. Shinoda et al. (1998) investigated the influence of the groove geometry, thereby concluding that a rounded section enabled a more effective deposition and fitting. Grooves with sharp edged cross sections did not ease the fitting between the substrate and the deposited material.

Fig. 48 depicts the production of cutting tools by embedding the friction surfaced coating in a channel milled in the substrate. This application will be addressed with further detail in section 9 of the present review.

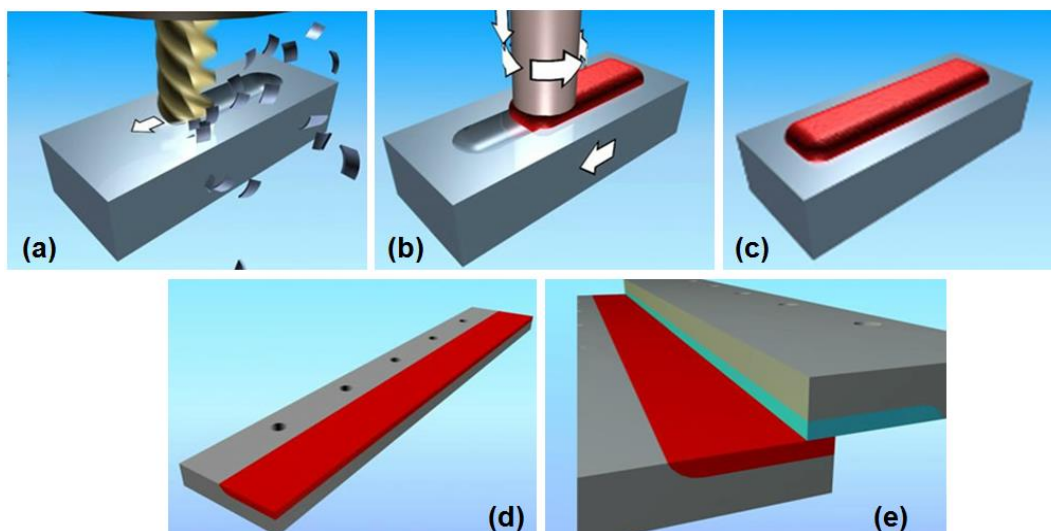


Fig. 48. Production of cutting tools based on FS. (a) Channel milled in preparation for FS inlay, (b) FS process being applied, (c) as-deposited coating, (d) post-processing into desirable geometry, (e) finished product. FRICTEC Inc. (Svarka, 2010).

The use of heat treatment has been investigated to enhance as-deposited mechanical properties. In an effort to develop alternative processing methods for high speed steels, Bedford et al. (2001) reported the use of tempering to induce secondary hardening on deposits produced by FS, comparing the resulting properties with the conventional production heat treatment process. As shown by Fig. 49, the abrupt thermal cycle provided by FS enables a faster production of a fine and homogenous distribution of carbides in the fully hardened state, equivalent to those produced by more recent powder manufacturing processes. The only post-coating heat treatment required is tempering, as in conventional hardened high-speed steels. The use of posterior heat treatment was also addressed by Macedo (2011).

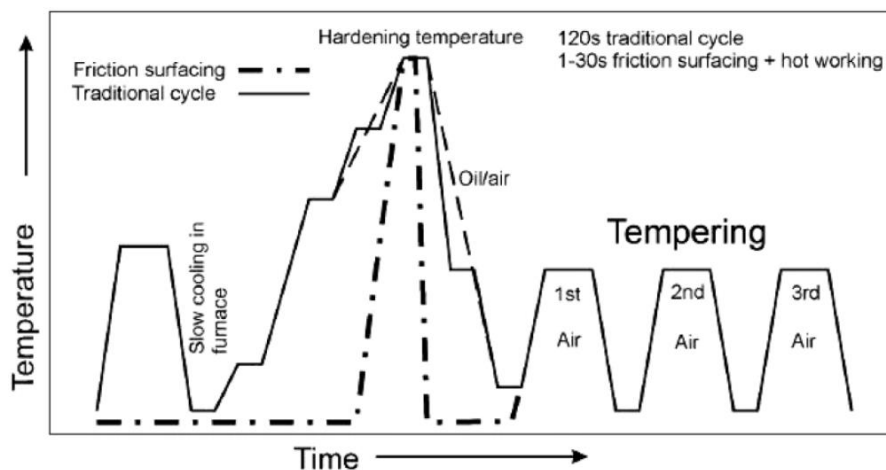


Fig. 49. Traditional heat treatment cycle of high speed steels and FS thermal cycle followed by traditional tempering (Bedford et al., 2001).

6.6. Composite production

The mechanisms involved in FS provide an alternative process to produce metal matrix composites (MMC), as the inherent severe plastic deformation can be used to promote the dispersion and mixture of reinforcement particles within the coating metal matrix. The composite layer becomes soundly bonded to the substrate while preserving its integrity. Tooling costs are not an issue and the metal matrix is solely provided by the consumable.

An example of application was patented by Thomas and Nicholas (1990) envisaging mainly the manufacturing of brake disks. Alloyed steel hollow consumable rods were packed with mixtures of hard particles as tungsten, cobalt, molybdenum, silicon carbide or titanium. FS was then performed, depositing a composite layer onto the disk substrates. The coatings produced by this method could display abrasive properties according to the part design.

Bedford et al. (1994) used the Osprey process to manufacture steel matrix composite bar stocks that were later used as consumable rods for FS. The coatings produced enabled a high degree of ceramic particle refinement, enhancing the original composite microstructure to present higher wear resistances.

Shinoda and Li (1999) explored the production of aluminium based MMC by packing an AA5052 hollow rod with alumina particles. Deposition was performed over an AA5083 plate, achieving a uniform distribution of reinforcements with a 12% volume fraction.

The use of alumina particle reinforcements to improve the wear resistance of AA6061 coatings has been investigated by Nakama et al. (2008a). More recently, Reddy et al. (2009) and Reddy et al. (2011) addressed the production of aluminium MMC coatings on aluminium and titanium substrates. The production of SiC reinforced AA2124 aluminium alloy coatings over A356 aluminium and Ti-6Al-4V titanium substrates, resulted in improved wear resistance, while corrosion resistance was reported as moderate.

Additionally, multi-layering will enable to tailor coating composition in order to achieve pre-defined gradients. By performing successive fully overlapped depositions with increasing SiC concentrations or particle size, a composition gradient was

achieved, as shown by Gandra et al. (2013b). The SiC area fraction was seen to vary from 5 to 30% along the thickness, reaching the maximum hardness of 110 HV at the coating surface (about 30% higher than the hardness of the depositions performed without particles). The use of SiC reinforcements resulted in improved wear performance of the AA6082 FS coatings, presenting a 13% lower wear rate.

Table 4 summarizes the investigations reported in literature addressing the manufacture of composites by FS.

Table 4. Investigations reporting the production of composites by FS.

Substrate	Coating		Application	Ref.
	Consumable rod	Reinforcement		
Aluminium				
- A356	AA2024	SiC	Wear and corrosion resistance	(Reddy et al., 2011; Reddy et al., 2009)
- AA5083	AA5052	Al ₂ O ₃	-	(Shinoda and Li, 1999)
- AA6061	AA6061	Al ₂ O ₃	Wear resistance	(Nakama et al., 2008a)
- AA2024	AA6082	SiC	Wear resistance	(Gandra et al., 2013b)
Titanium				
- Ti-6Al-4V	AA2024	SiC	Wear and corrosion resistance	(Reddy et al., 2011; Reddy et al., 2009)
Alloy steel	Alloy steel	W, Co, SiC, Mo or Ti.	Wear resistance	(Bedford et al., 1994; Thomas and Nicholas, 1990)

7. Advantages and disadvantages

FS is best suited for applications requiring joining of materials with compatibility issues or which are not easily processed by fusion processes. The process involves a hot forging action, which refines significantly the microstructure of the deposited material. The deposit is inherently homogenous and presents attractive mechanical properties.

Coating technologies based on fusion welding processes as laser cladding, shielded metal arc welding or plasma transferred arc surfacing, often struggle with defects commonly associated to casting mechanisms and high temperature exposure. These defects are not observed in FS, as the coating results from viscoplastic deformation.

Considering other solid state cladding processes, such as, explosive cladding or roll bonding, FS can be seen as a more versatile alternative for localized treatments.

Rao et al. (2012a) compared the microstructure and hardness of Stellite6 coatings produced by FS with those produced by fusion based processes, such as, gas tungsten arc and plasma transferred arc welding. Friction surfaced coatings presented a finer microstructure and relatively higher hardness values (Fig. 50). The absence of a solidification structure and chemical homogeneity was also referred as advantages associated with the FS process.

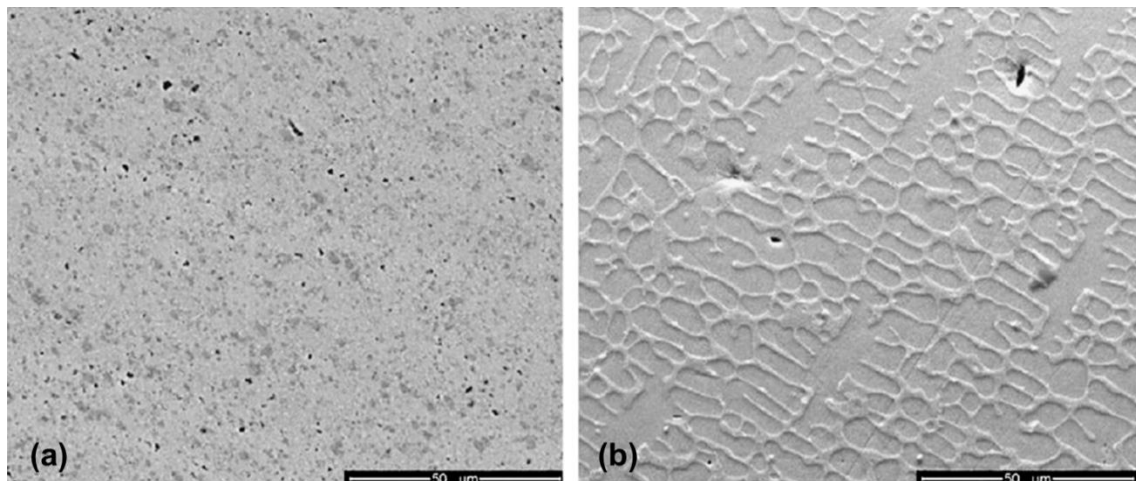


Fig. 50. Microstructures of Stellite6 coatings a) friction surfaced, b) gas tungsten arc (Rao et al., 2012a).

Similar findings were presented by Puli and Janaki Ram (2012a) regarding corrosion resistance. Friction surfaced AISI 316 stainless steel coatings presented superior corrosion resistance in comparison with those produced by manual arc welding processes, being invulnerable to intergranular corrosion.

The absence of melting makes FS a very promising technique to process materials with lower melting temperatures, such as, aluminium and magnesium alloys. As highlighted

by Kramer de Macedo et al. (2010), the absence of spatter, radiation emissions or fumes makes FS a cleaner and more environmental friendly technology.

However, FS struggles with several technical and productivity issues which contribute to a limited range of engineering applications. One of the main process disadvantages is the poor bonding at the coating edges, as post-processing operations are often required to remove them. The usable bond width is less than the width of the coating produced, as was described by Voutchkov et al. (2001) (Fig. 51).

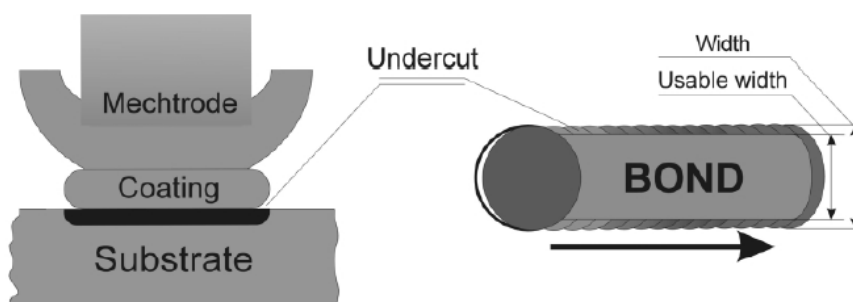


Fig. 51. Usable bond and undercut definition, as defined by Voutchkov et al. (Voutchkov et al., 2001).

Moreover, the generation of a revolving flash at the consumable rod tip contributes to a decrease in mass transfer efficiency, as it represents material that does not bond to the substrate. FS enables a limited control over the deposited thickness and width, as coating geometry is determined by a relatively narrow range of process parameters. Several authors describe the use of consumable rods from 2 up to 32 mm in diameter. Depending on the process parameters, consumable rod diameter and material, coating thickness is typically between 0.2 and 3 mm, as reported by Voutchkov et al. (2001).

8. Performance analysis

FS analytic performance criteria regarding the material deposition rate and specific energy consumption were recently established, thereby contributing to a realistic comparison with other coating technologies.

8.1. Material transfer

Volumetric rod consumption rate (CR_{vol}) is determined by multiplying the rod plunging speed (V_z) by its cross section area (A_r), where r is the rod radius, using the following Eq. (5).

$$CR_{vol}[m^3/s] = A_r V_z = \pi r^2 V_z \quad (5)$$

Likewise, the product between the travel speed (v) and the deposited cross section area (A_d) expresses the volumetric deposition rate (DR_{vol}) throughout the FS process, as given by Eq. (6).

$$DR_{vol}[m^3/s] = A_d v \quad (6)$$

Considering the consumable rod material density (ρ), CR and DR can be rewritten in order to express the mass flow, as depicted by Eq. (7) and (8).

$$CR[kg/s] = CR_{vol} \cdot \rho \quad (7)$$

$$DR[kg/s] = DR_{vol} \cdot \rho \quad (8)$$

In order to determine the fraction of consumed material deposited and that is transferred to flash, the deposition efficiency ($\eta_{deposition}$) can be defined as the ratio between DR and CR , as given by Eq. (9).

$$\eta_{deposition} = \frac{DR}{CR} \quad (9)$$

However, due to the formation of side unbonded regions, just a part of the deposited material is effectively joined. As such, the joining efficiency ($\eta_{joining}$) is given by the ratio between the bonded width (W_b) and the maximum coating width (W_d), as expressed by Eq. (10)

$$\eta_{joining} = \frac{W_b}{W_d} \quad (10)$$

Thus, the effective coating efficiency ($\eta_{coating}$) reflects the fraction of consumed rod that actually becomes bonded to the substrate and is estimated by multiplying Eq. (9) and (10), thereby obtaining Eq. (11).

$$\eta_{coating} = \eta_{deposition} \cdot \eta_{joining} = \frac{A_d v}{\pi r^2 V_z} \cdot \frac{W_b}{W_d} \quad (11)$$

8.2. Energy consumption

The mechanical power supplied by the equipment (\dot{W}_e) can be divided into three main contributions regarding rod rotation (\dot{W}_r), axial plunging (\dot{W}_z) and travel (\dot{W}_x), as determined by Eq. (12).

$$\dot{W}_e [J/s] = \dot{W}_r + \dot{W}_z + \dot{W}_x = \frac{2\pi\Omega}{60} T + F_z V_z + F_x v \quad (12)$$

Hence, energy consumption per deposited unit of mass or specific energy consumption (EC) as given by Eq. (13):

$$EC [J/kg] = \dot{W}_e / DR \quad (13)$$

In the deposition of mild steel, FS was seen to require mechanical work between 2.5 and 5 kJ per gram of deposited coating with deposition rates from 0.5 to 1.6 g/s (Gandra et al., 2012). Shinoda et al. (1996) reported a top deposition rate of 0.28 g/s using martensitic stainless steel AISI 440 rods and structural steel plates. Thomas (1987) reported a deposition rates of 1.38 g/s and 1.94 g/s, when depositing austenitic stainless steel and mild steel respectively. Deposition rates are similar to laser cladding and plasma arc welding, while specific energy consumption is lower than for other arc-welding processes, as reported both by Shinoda et al. (1996). Regarding deposition efficiency, flash formation accounted for 40 to 60% of the overall consumable rod consumption, in the deposition of mild steel (Gandra et al., 2012). Tokisue et al. (2006) and Sakihama et al. (2003) reported deposition efficiencies from 20 to 40% in the FS of

similar and dissimilar combinations of aluminium alloys. Similar values were reported by Nakama et al. (2008b) in the FS of magnesium alloys.

9. Case studies and industrial applications

FS allows assembling in a single component tailored material property combinations which are difficult to gather by a single material. By adding the required material properties according to the different loading areas of the part, the use of more expensive materials, capable of assembling all functional requirements, can be avoided.

Since the original concept presented by Klopstock and Neelands (1941) there are several reports on case studies, mainly in the rehabilitation of worn or damaged parts, as well as, in the production of wear and corrosion resistant coatings. FS has been investigated to repair shafts and agricultural parts (Nogik, 1970; Thomas, 1988; Tyayar, 1959; Zakson and Turukin, 1965). Case studies addressing bronze and steel combinations also suggest possible applications in the production of sliding tiles or the restoring of bushings for bearings and rolling joints (Kershenbaum, 1972; Kershenbaum and Averbukh, 1964; Kershenbaum and Averbukh, 1972).

In the 90's the process saw its first successful commercial application, as a hard facing technology for the manufacturing of cutting tools and punches. This particular FS method was patented by Bedford and Richards (1990), one of the founders of the company currently exploring this application, FRICTEC Ltd. Various configurations are exemplified, featuring the deposition of Stellite 6 and high speed tool steels on mild steel and stainless steel substrates. This company focuses on the production of cutting edges for guillotines, blades and knives for the fast moving consumer goods processing and packing industry (Fig. 48). Their approach can also be adapted to form edge faces for

screw drivers, chisels and valve seats. The parts present a strong resistance to delamination.

Another application features the hard facing and repair of gas turbine blade tips. In a case study presented by Bedford et al. (1995), single and multi-layer coatings of Stellite 12 were produced along narrow substrates of stainless steel AISI 316 to simulate the deposition along a blade edge (Fig. 52). Localized repairs were also explored. A similar procedure was proposed by Amos (1993) for hard facing steam turbine blade trailing edges, as shown by Fig. 53. Foster et al. (1996) described a method to perform circumferential depositions around disks or drums, from which a set of several compressor or turbine blades could be extracted.

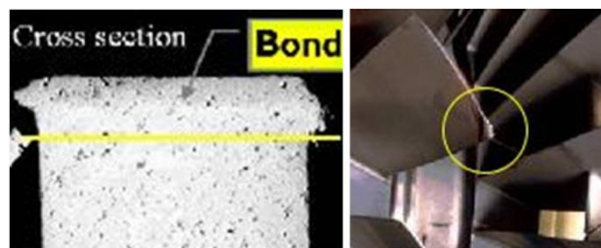


Fig. 52. Repair of turbine blade tips by FS. (a) Cross section of a deposit onto a blade tip and (b) repaired blade (Bedford et al., 1995).

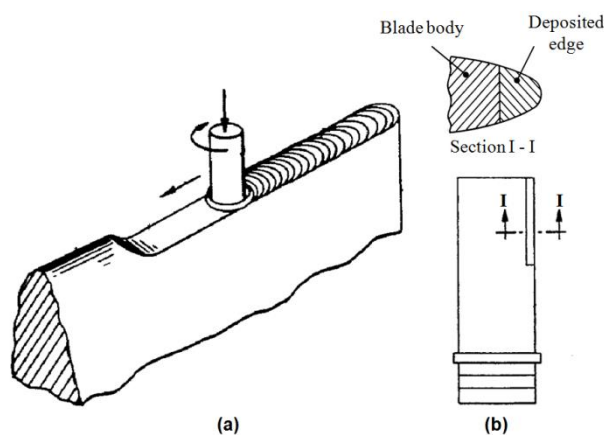


Fig. 53. Method of forming a trailing edge on a steam turbine blade. (a) Deposition configuration and (b) section view evidencing the finished part (Amos, 1993).

The surfacing of pipe flange contact faces, brake disks, the repair of anode bars and the hermetic sealing of containers has also been reported as promising applications by Dunkerton and Thomas (1984). Govardhan et al. (2012) suggested potential uses in the manufacture of petrochemical pressure vessels or pumps for chemicals, based on the corrosion performance studies of austenitic stainless steel deposits over mild steel. FS can also be applied in the context of surface recovery in underwater environments, such as, offshore pipes and structures, as shown by Li and Shinoda (2000), including the possibility of use under harsh weather conditions.

Yamashita and Fujita (2001) demonstrated the feasibility of performing the in-situ repair of components damaged by stress corrosion cracking at nuclear power plants. FS allowed a lower heat input, while avoiding the detrimental tensile residual stresses as those induced by fusion welding conventional alternatives. By performing a shallow gridding preparation step, surface cracks could be sealed by a FS deposition.

Beyer et al. (2003) showed that tridimensional depositions are consistent with results obtained for linear horizontal paths. Fig. 54 depicts the repair test of a cylindrical part with 400 mm radius using a Tricept TR 805 robot. This particular robot model was stiff enough to endure the forces involved and guarantee the process dynamic stability.

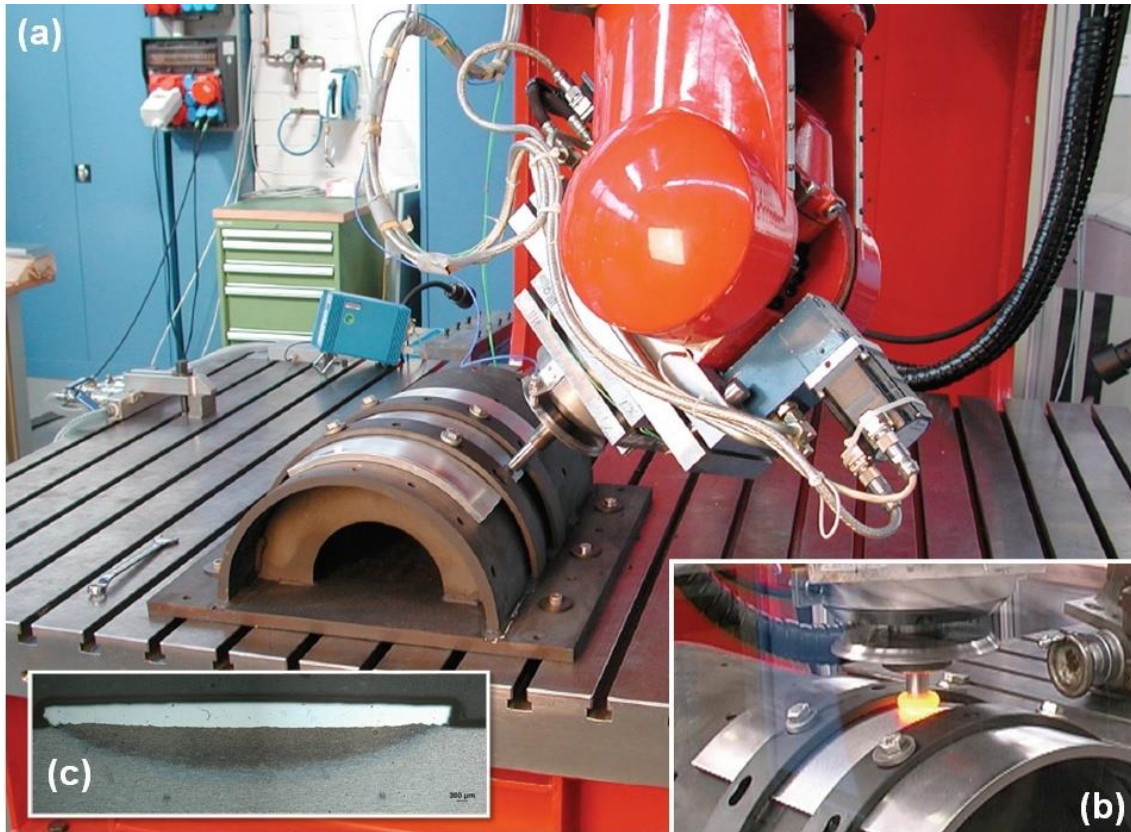


Fig. 54. FS of stainless Steel on a mild steel cylindrical part using a Tricept TR805 robot. (a) Setup and clamping system, (b) deposition, (c) cross section macrograph of coating (Beyer et al., 2003).

FS has also been investigated for the in-situ reclamation of worn railway trails. As shown by Fig. 55, Doughty et al. (2009) developed a dedicated portable system for performing repairs on site, thereby reducing the costs of removing or interrupting railway circulation. The system is fixed directly on the rail, providing the basis to apply the consumable rod axial load, as well as, the travel movement along the longitudinal direction. This solution also considered the angular adjustment of the consumable rod in order to perform depositions along the different regions of interest on the rail.

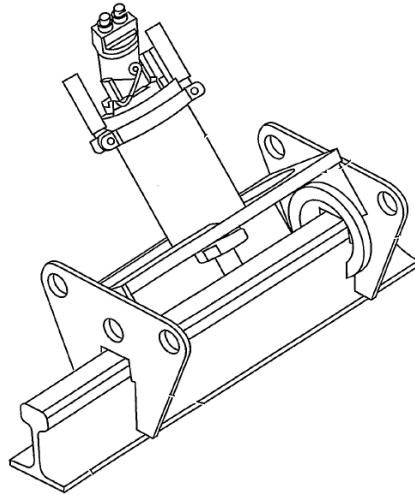


Fig. 55. Device for treating rails in-situ (Doughty et al., 2009).

10. Summary and future outlook

In this paper a comprehensive review on the friction surfacing technology is presented, addressing the following aspects: fundamentals of the process, influence of process parameters, microstructural transformations, technology developments, performance analysis, case studies and industrial applications.

The process is based on the hot forging action of a rotating consumable rod that, refining the microstructure of the deposited material. The establishment of a starting condition in terms of torque, applied axial force, travel and rotation speeds is very important for a successful deposition of material onto a substrate.

FS is a coating technology mainly suitable for localized surface engineering applications, requiring the joining of materials with compatibility issues. As a solid state process, there is no bulk melting involved, which results in lower residual stress levels and avoids the degradation of base material properties. The absence of splashes, toxic fumes and radiation also makes FS a cleaner alternative. Recent investigations emphasize its competitiveness as far as energy efficiency is concerned.

Extensive research has been published on its capability of producing homogenous and fine grained microstructures, which can yield attractive mechanical properties. With special focus on the manufacturing of long-life cutting tools, it has been used for hard facing, anti-corrosion coating and in the repair of damaged parts from agricultural machinery to turbine blades. However, bonding quality at coating edges is generally poor and post processing is required to machine the coating into the desired geometry. For the same reason, this technique has limited overlay capabilities, limiting its use for spot or linear coating operations.

With a relative extended research addressing steel alloy combinations, it is foreseen that future investigations will continue to advance to more ambitious dissimilar combinations. The number of investigations addressing this process is still increasing pushed by the crescent industrial demand for higher performance of materials with dedicated surface properties. Research addressing copper, brass, magnesium and titanium is relatively scarce compared to the number of studies addressing steel and aluminium alloys. The most successful investigations up to date feature dissimilar combinations of aluminium alloys, as well as, the deposition of tool steels and stainless steels over mild steel substrates. Bonding has been reported to rely on the combined effect of interfacial diffusion and mechanical locking.

In spite of several attempts to model FS, ultimate process parameter selection is still mainly based on empirical knowledge. Most existing models account for a limited number of case scenarios when considering the vast number of potential applications. Future research will continue to address the material flow and thermal modelling of the process, as well as, parameter optimization models relying on neural networks or fuzzy logic.

Although FS requires the application of an axial load on the consumable, the process does not necessarily require load controlled machines. The use of conventional CNC machines has been suggested as key solution to increase the commercial viability of FS in industrial applications, restricting the use of more extensive load-controlled equipment for research and development. There is also a demand for rod continuous feeding systems, which would replace the need to interrupt the process to load new consumables. The use of cooling and flash-cutting systems is also seen as promising developments to increase process efficiency.

The technology has an enormous potential and is developing to overcome still existing problems. The advantages inherent to solid state processing are the driving force for its application and future research.

Acknowledgements

The authors would like to acknowledge FCT/MCTES funding for the project:

Technology developments of friction stir processing to produce functionally graded materials and improve surfaces for advanced engineering applications (PTDC/EME-TME/103543/2008 - FRISURF). JG acknowledges FCT/MCTES for funding its PhD grant SFRH/BD/78539/2011. RM acknowledges Pest OE/EME/UI0667/2011.

References

Amos, D.R., 1993. Method of forming a trailing edge on a steam turbine blade and the blade made thereby, US Patent No. 5183390 A.

Batchelor, A.W., Jana, S., Koh, C.P., Tan, C.S., 1996. The effect of metal type and multi-layering on friction surfacing. *Journal of Materials Processing Technology* 57, 172-181. doi: 10.1016/0924-0136(95)02057-8.

Bedford, G.M., 1991. Friction surfacing a rotating hard metal facing material onto a substrate material with the benefit of positively cooling the substrate, US Patent No. 5077081 A.

Bedford, G.M., Richards, P.J., 1985. On the absence of dilution in friction surfacing and later friction welding, 1st International Conference on Surface Engineering, Brighton, pp. 279-290.

Bedford, G.M., Richards, P.J., 1990. Method of forming hard facings on materials, US Patent No. 4930675 A.

Bedford, G.M., Sharp, R.J., Davis, A.J., 1995. Micro-friction surfacing in the manufacture and repair of gas turbine blades. 3rd International Charles Parsons Turbine Conference: Materials Engineering in Turbines and Compressors, Newcastle Upon Tyne, 689-698.

Bedford, G.M., Sharp, R.P., Wilson, B.J., Elias, L.G., 1994. Production of friction surfaced components using steel metal matrix composites produced by Osprey process. *Surface Engineering* 10, 118-122.

Bedford, G.M., Vitanov, V.I., Voutchkov, I.I., 2001. On the thermo-mechanical events during friction surfacing of high speed steels. *Surface and Coatings Technology* 141, 34-39. doi: 10.1016/S0257-8972(01)01129-X.

Beyer, M., Resende, A., Santos, J.F.d., 2003. Friction surfacing for multi-sectorial applications - FRICSURF, Institute for Materials Research, GKSS Forschungszentrum Geesthacht GmbH, Technical report.

Bishop, E., 1960. Friction welding in the Soviet union. *Welding and Metal Fabrication*, 408-410.

Chandrasekaran, M., Batchelor, A.W., Jana, S., 1998. Study of the interfacial phenomena during friction surfacing of mild steel with tool steel and inconel. *Journal of Materials Science* 33, 2709-2717. doi: 10.1023/A:1004338210262.

Chandrasekaran, M., William Batchelor, A., Jana, S., 1997. Friction surfacing of metal coatings on steel and aluminum substrate. *Journal of Materials Processing Technology* 72, 446-452. doi: 10.1016/S0924-0136(97)00209-4.

Doughty, R.W., Shaw, D.J., Gibson, D.E., 2009. Friction stir surfacing process and device for treating rails, Patent No. WO 2009030960 A1.

Dunkerton, S.B., Thomas, W.M., 1984. Repair by friction welding. Repair and Reclamation, London,

Foster, D.J., Gillbanks, P.J., Moloney, K.C., 1996. Integrally bladed disks or drums, US Patent No. 5556257 A.

Fukakusa, K., 1996. On the characteristics of the rotational contact plane - a fundamental study of friction surfacing. *Welding International* 10, 524-529. doi: 10.1080/09507119609549043.

Gandra, J., Miranda, R.M., Vilaça, P., 2011. Monitoring of temperature and mechanical parameters in friction surfacing. IIW 2011 - 64th Annual Assembly, Commission III-1592-11, Chennai,

Gandra, J., Miranda, R.M., Vilaça, P., 2012. Performance analysis of friction surfacing. *Journal of Materials Processing Technology* 212, 1676-1686. doi: 10.1016/j.jmatprotec.2012.03.013.

Gandra, J., Pereira, D., Miranda, R.M., Silva, R.J.C., Vilaça, P., 2013a. Deposition of AA6082-T6 over AA2024-T3 by friction surfacing - Mechanical and wear characterization. *Surface and Coatings Technology* 223, 32-40. doi: 10.1016/j.surfcoat.2013.02.023.

Gandra, J., Vigarinho, P., Pereira, D., Miranda, R.M., Velhinho, A., Vilaça, P., 2013b. Wear Characterization of Functionally Graded Al-SiC Composite Coatings Produced by Friction Surfacing. *Materials & Design*. doi: 10.1016/j.matdes.2013.05.059.

Govardhan, D., Kumar, A.C.S., Murti, K.G.K., Madhusudhan Reddy, G., 2012. Characterization of austenitic stainless steel friction surfaced deposit over low carbon steel. *Materials & Design* 36, 206-214. doi: 10.1016/j.matdes.2011.07.040.

Hanke, S., Fischer, A., Beyer, M., dos Santos, J., 2011. Cavitation erosion of NiAl-bronze layers generated by friction surfacing. *Wear* 273, 32-37. doi: 10.1016/j.wear.2011.06.002.

Hanlon, T., Fritz, J.B., Bernath, J.J., Channell, A.B., Blank, J.P., Kalabekov, S.E., Hootman, J.R., Trapp, T.J., 2010. Apparatus and method for friction surfacing using a consumable pin tool, US Patent No. 8056793 B2.

Jaworski, B., Voutchkov, I.I., Vitanov, V.I., Hughes, V., 2000. Modelling of the Friction Surfacing Process for Turbine Blade Reclamation. *Proceedings of the 33rd International MATADOR Conference*, 307-312.

Jenkins, B.M., Doyle, E.D., 1987. Advances in friction deposition – Low-pressure friction surfacing. *International Tribology Conference, Melbourne*, 87-94.

Jenkins, B.M., Doyle, E.D., 1989. Hardfacing by low-pressure friction surfacing. Transactions of the Institution of Engineers, Australia. Mechanical engineering ME14, 178-185.

Kalken, A.M., 2001. Friction surfacing of stainless steel on mild steel with a robot, Master Thesis, Delft University of Technology.

Katayama, Y., Takahashi, M., Shinoda, T., Nanbu, K., 2009. New friction surfacing application for stainless steel pipe. Welding in the world 53, 272-280.

Kershenbaum, V.Y., 1972. Performance of steel bronze bimetal produced by friction surfacing. Svar. Proizvod. 7, 29-30.

Kershenbaum, V.Y., Averbukh, B.A., 1964. Special features in the friction deposition of bronze on steel. Avesta Svarka 3, 19-22.

Kershenbaum, V.Y., Averbukh, B.A., 1972. Optimum dimensions of friction surfaced components. Avesta Svarka 5, 64-66.

Klopstock, H., Neelands, A.R., 1941. An improved method of joining or welding metals, UK Patent No. GB572789.

Kramer de Macedo, M.L., Pinheiro, G.A., dos Santos, J.F., Strohaecker, T.R., 2010. Deposit by friction surfacing and its applications. Welding International 24, 422-431. doi: 10.1080/09507110902844535.

Krohn, H., 2010. Temperaturmanagement des Reibauftragschweißens, Master Thesis, Technische Universität Hamburg-Harburg.

Lambrineas, P., Jenkins, B.M., Doyle, E.D., 1990. Low-pressure friction surfacing: adhesion of stainless steel coatings on mild steel. International Tribology Conference, Brisbane, 12-15.

Lambrineas, P., Jewsbury, P., 1992. Areal coverage using friction surfacing. Journal of Ship Production 8, 131-136.

- Li, J.Q., Shinoda, T., 2000. Underwater friction surfacing. *Surface Engineering* 16, 31-35. doi: 10.1179/026708400322911483.
- Liu, X., Yao, J., Wang, X., Zou, Z., Qu, S., 2009. Finite difference modeling on the temperature field of consumable-rod in friction surfacing. *Journal of Materials Processing Technology* 209, 1392-1399. doi: 10.1016/j.jmatprotec.2008.03.067.
- Liu, X.M., Zou, Z.D., Zhang, Y.H., Qu, S.Y., Wang, X.H., 2008. Transferring mechanism of the coating rod in friction surfacing. *Surface and Coatings Technology* 202, 1889-1894. doi: 10.1016/j.surfcoat.2007.08.024.
- Ma, Z.Y., 2008. Friction stir processing technology: A review. *Metallurgical and Materials Transactions A* 39A, 642-658. doi: 10.1007/s11661-007-9459-0.
- Macedo, M.L.K., 2011. Caracterização de depósitos realizados pelo processo de deposição por fricção em chapas de aço de alto carbono, PhD Thesis, Universidade Federal do Rio Grande do Sul.
- Mishra, R.S., Ma, Z.Y., 2005. Friction stir welding and processing. *Materials Science and Engineering: R: Reports* 50, 1-78. doi: 10.1016/j.mser.2005.07.001.
- Nakama, D., Katoh, K., Tokisue, H., 2008a. Fabrication of 6061 aluminum alloy/Al₂O₃ particle composites by friction surfacing. *Journal of Japan Institute of Light Metals* 58, 299-304. doi: 10.2464/jilm.58.299.
- Nakama, D., Katoh, K., Tokisue, H., 2008b. Some characteristics of AZ31/AZ91 dissimilar magnesium alloy deposit by friction surfacing. *Materials Transactions* 49, 1137-1141.
- Nicholas, E.D., 1993. Friction Surfacing, In: Olson, D., Siewert, T., Liu, S., Edwards, G. (Eds.), *ASM Handbook - Welding Brazing and Soldering*. ASM International, pp. 321-323.
- Nicholas, E.D., 2003. Friction processing technologies. *Welding in the World* 47, 2-9.

Nicholas, E.D., Thomas, W.M., 1986. Metal deposition by friction welding. *Welding Journal*, 17-27.

Nogik, M.V., 1970. Friction hardfacing steel with stellite v3k. *Svar. Proizvod.* 8, 16-17.

Pratt, A.J.S., 1995. Apparatus for continuous axial feeding of an elongate member, US Patent No. 5419480 A.

Puli, R., Janaki Ram, G.D., 2012a. Corrosion performance of AISI 316L friction surfaced coatings. *Corrosion Science* 62, 95-103. doi: 10.1016/j.corsci.2012.04.050.

Puli, R., Janaki Ram, G.D., 2012b. Microstructures and properties of friction surfaced coatings in AISI 440C martensitic stainless steel. *Surface and Coatings Technology* 207, 310-318. doi: 10.1016/j.surfcoat.2012.07.001.

Puli, R., Kumar, E.N., Ram, G.D.J., 2011. Characterization of friction surfaced martensitic stainless steel (AISI 410) coatings. *Transactions of The Indian Institute of Metals* 64, 41-45.

Rafi, H.K., Balasubramaniam, K., Phanikumar, G., Rao, K.P., 2011a. Thermal profiling using infrared thermography in friction surfacing. *Metallurgical and Materials Transactions A* 42, 3425-3429.

Rafi, H.K., Phanikumar, G., Prasad Rao, K., 2011b. Material Flow Visualization during Friction Surfacing. *Metallurgical and Materials Transactions A* 42, 937-939. doi: 10.1007/s11661-011-0614-2.

Rafi, H.K., Ram, G.D.J., Phanikumar, G., Rao, K.P., 2010a. Friction surfaced tool steel (H13) coatings on low carbon steel: A study on the effects of process parameters on coating characteristics and integrity. *Surface and Coatings Technology* 205, 232-242. doi: 10.1016/j.surfcoat.2010.06.052.

Rafi, H.K., Ram, G.D.J., Phanikumar, G., Rao, K.P., 2010b. Friction surfacing of austenitic stainless steel on low carbon steel: Studies on the effects of traverse speed, World Congress on Engineering 2010, London.

Rafi, H.K., Ram, G.D.J., Phanikumar, G., Rao, K.P., 2011c. Microstructural evolution during friction surfacing of tool steel H13. *Materials and Design* 32, 82-87. doi: 10.1016/j.matdes.2010.06.031.

Rao, K.P., Damodaram, R., Rafi, H.K., Ram, G.D.J., Reddy, G.M., Nagalakshmi, R., 2012a. Friction surfaced Stellite6 coatings. *Materials Characterization* 70, 111-116. doi: 10.1016/j.matchar.2012.05.008.

Rao, K.P., Sankar, A., Rafi, H.K., Ram, G.D.J., Reddy, G.M., 2012b. Friction surfacing on nonferrous substrates: a feasibility study. *International Journal of Advanced Manufacturing Technology*.

Rao, K.P., Sreenu, A.V., Rafi, H.K., Libin, M.N., Balasubramaniam, K., 2012c. Tool steel and copper coatings by friction surfacing – A thermography study. *Journal of Materials Processing Technology* 212, 402-407. doi: 10.1016/j.jmatprotec.2011.09.023.

Ravi, A.M., 2011. Investigation of friction surfacing parameters for the improvement of wear properties of AA 6082 coatings on AA 2024, Master Thesis, Technische Universität Hamburg-Harburg.

Reddy, G.M., Prasad, K.S., Rao, K.S., Mohandas, T., 2011. Friction surfacing of titanium alloy with aluminium metal matrix composite. *Surface Engineering* 27, 92-98. doi: 10.1179/174329409X451128.

Reddy, G.M., Rao, K.S., Mohandas, T., 2009. Friction surfacing: Novel technique for metal matrix composite coating on aluminium silicon alloy. *Surface Engineering* 25, 25-30. doi: 10.1179/174329408X298238.

Sakihama, H., Tokisue, H., Katoh, K., 2003. Mechanical properties of friction surfaced 5052 aluminum alloy. *Materials Transactions* 44, 2688-2694.

Shinoda, T., Li, J., 1999. Surface modification of 5083 aluminum alloys using friction surfacing. *Journal of Japan Institute of Light Metals* 49, 499-503.

Shinoda, T., Li J, Q., Katoh, Y., Yashiro, T., 1998. Effect of process parameters during friction coating on properties of non-dilution coating layers. *Surface engineering* 14, 211-216.

Shinoda, T., Okamoto, S., Takemoto, S., Kato, Y., Shimizu, T., 1996. Deposition of hard surfacing layer by friction surfacing. *Welding International* 10, 288-294. doi: 10.1080/09507119609548997.

Shirzadi, A.A., Assadi, H., Wallach, E.R., 2001. Interface evolution and bond strength when diffusion bonding materials with stable oxide films. *Surface and Interface Analysis* 31, 609-618.

Sugandhi, V., Ravishankar, V., 2012. Optimization of friction surfacing process parameters for aa1100 aluminum alloy coating with mild steel substrate using response surface methodology (rsm) technique. *Modern Applied Science* 6, 69-80.

Suhuddin, U., Mironov, S., Krohn, H., Beyer, M., Dos Santos, J.F., 2012.

Microstructural evolution during friction surfacing of dissimilar aluminum alloys.

Metallurgical and Materials Transactions A: Physical Metallurgy and Materials Science 1-8.

FRICTEC, 2012. <http://www.frictec.co.uk>.

Thomas, W.M., 1988. Solid phase cladding by friction surfacing. *TWI International Symposium, Cambridge*, 18.

Thomas, W.M., 2009a. An Investigation and Study into Friction stir Welding of Ferrous-Based Material, PhD Thesis, University of Bolton.

- Thomas, W.M., 2009b. An Investigation and Study into Friction stir Welding of Ferrous-Based Material, University of Bolton.
- Thomas, W.M., Nicholas, E.D., 1990. Surfacing method, US Patent No. 4959241 A.
- Thomas, W.M., Nicholas, E.D., Watts, E.R., Staines, D.G., 2002. Friction based welding technology for aluminium. The 8 th International Conference on Aluminium Alloys, Cambridge, 1543-1548.
- Thomas, W.N., 1987. Friction surfacing. 2nd international conference on Flash-butt and friction welding, 124-140.
- Tokisue, H., Katoh, K., Asahina, T., Usiyama, T., 2006. Mechanical properties of 5052/2017 dissimilar aluminum alloys deposit by friction surfacing. *Materials Transactions* 47, 874-882.
- Tyayar, K.H.A., 1959. Friction welding in the reconditioning of worn components. *Svar. Proizvod.* 1, 3-24.
- Verevkin, V.I., Druchinin, S.A., Koshelev, A.A., 2003. Calculation of parameters of friction surfacing regimes on basis of mathematical modeling. *Izvestiya Vysshikh Uchebnykh Zavedenii, Chernaya Metallurgiya* 6, 50-53.
- Vilaça, P., Gandra, J., Vidal, C., 2012. Linear friction based processing technologies for aluminum alloys: Surfacing, stir welding and stir channeling, In: Ahmad, Z. (Ed.), *Aluminium Alloys - New Trends in Fabrication and Applications*. InTech.
- Vitanov, V.I., Javaid, N., 2010. Investigation of the thermal field in micro friction surfacing. *Surface and Coatings Technology* 204, 2624-2631. doi: 10.1016/j.surfcoat.2010.02.003.
- Vitanov, V.I., Javaid, N., Stephenson, D.J., 2010. Application of response surface methodology for the optimisation of micro friction surfacing process. *Surface and Coatings Technology* 204, 3501-3508. doi: 10.1016/j.surfcoat.2010.04.011.

- Vitanov, V.I., Voutchkov, I.I., 2005. Process parameters selection for friction surfacing applications using intelligent decision support. *Journal of Materials Processing Technology* 159, 27-32. doi: 10.1016/j.jmatprotec.2003.11.006.
- Vitanov, V.I., Voutchkov, I.I., Bedford, G.M., 2000. Decision support system to optimise the Frictec (friction surfacing) process. *Journal of Materials Processing Technology* 107, 236-242. doi: 10.1016/S0924-0136(00)00710-X.
- Vitanov, V.I., Voutchkov, I.I., Bedford, G.M., 2001. Neurofuzzy approach to process parameter selection for friction surfacing applications. *Surface and Coatings Technology* 140, 256-262. doi: 10.1016/S0257-8972(01)01128-8.
- Voutchkov, I., Jaworski, B., Vitanov, V.I., Bedford, G.M., 2001. An integrated approach to friction surfacing process optimisation. *Surface and Coatings Technology* 141, 26-33. doi: 10.1016/S0257-8972(01)01127-6.
- Yamashita, H., Fujita, K., 2001. Newly developed repairs on welded area of LWR stainless steel by friction surfacing. *Journal of Nuclear Science and Technology* 38, 896–900.
- Yao, J.S., 2001. A study on the physical process of consumable-rod friction welding, PhD Thesis, Beijing University of Aeronautics and Astronautics.
- Zakson, R.I., Turukin, F.G., 1965. Friction welding and hardfacing of agricultural machine parts. *Avesta Svarka* 3, 48-50.
- Zhang, Z.R., Xiao, X.T., Liu, Y.F., Xue, K.M., 1997. Coupled thermo-mechanical FEM analysis of twist-compression deformation. *Transactions of Nonferrous Metals Society of China* 7, 102-106.

Figure captions

Fig. 1. Friction surfacing of an AA6082-T6 aluminium alloy over AA2024-T3. (a) Rotation start, (b) initial contact, (c) initial deformation stage and (d) deposition stage.

Fig. 2. Thermo-mechanical events in the FS of high speed steels (Bedford et al., 2001).

Fig. 3. Cross-section showing coating/substrate interface. FS of AISI 316 stainless steel on a mild steel substrate. (a) Fully bonded interface at coating center, (b) undercut region at the coating edge (Vitanov et al., 2000).

Fig. 4. Typical top view of FS deposits. (a) AISI H13 over AISI 1020 (Rafi et al., 2010a), (b) AA2017 over AA5052 (Tokisue et al., 2006), (c) AISI 310 over AISI 1020 (Rafi et al., 2010b).

Fig. 5. Deposition process of mild steel over mild steel. Nomenclature: AS - advancing side, RS - retreating side (Gandra et al., 2012).

Fig. 6. Study of material flow in FS using a tracer marking technique. Top view X-ray radiographs revealing tracer distribution. Hole filled with tracers was placed at rod centre (Rafi et al., 2011b).

Fig. 7. Comparison between (a) the AISI H13 original rod microstructure and (b) the as-deposited condition, provided by SEM analysis. FS of AISI H13 tool steel over mild steel (Rafi et al., 2010a).

Fig. 8. Vickers microhardness profile across the coating/substrate interface (Rafi et al., 2011c).

Fig. 9. SEM observation of AISI 440C coating microstructure (Puli and Janaki Ram, 2012b).

Fig. 10. Typical microstructures of AISI 316L coating. (a) Optical, (b) TEM (Puli and Janaki Ram, 2012a).

Fig. 11. Microstructural transformations during the FS of AA6082-T6 over AA2024-T3. (a) Consumable base material, (b) Heat affected zone, (c) Compression-driven TMAZ,

(c) Torsion-driven TMAZ (e-f) Fully recrystallized microstructure, (g) Deposited material, (h) Bonding interface (Vilaça et al., 2012).

Fig. 12. Coating microstructure (a) and bonding interface (b) in the FS of AA6082-T6 over AA2024-T3 (Gandra et al., 2013b).

Fig. 13. Microstructural details in the FS of AZ91 over AZ31 (Nakama et al., 2008b).

Fig. 14. FS of Titanium 6.4 consumable rod and plate. (a) Coating microstructure and (b) push-off characterization (Beyer et al., 2003).

Fig. 15. Cavitation erosion study of NiAl-bronze layers generated by FS. (a) Microstructure of a friction surfaced sample. (b) coating close to surface, (c) coating close to substrate, (d) Coating production (Beyer et al., 2003), (e) Weight loss per worn area vs. cavitation test duration (Hanke et al., 2011).

Fig. 16. Tensile testing of AA5052 PH-34 deposits. (a) Sample extraction. Macrofractographs of tensile tested specimens produced using contact pressures of (b) 25 MPa and (c) 40 MPa (Sakihama et al., 2003).

Fig. 17. Scanning electron micrograph of several material combinations produced by FS. (a) tool steel AISI 01 / mild steel AISI 1020, (b) Inconel 600 / mild steel AISI 1020, (c) mild steel AISI 1020, (d) Stainless steel AISI 304 / AA5083 aluminium alloy (Chandrasekaran et al., 1998; Chandrasekaran et al., 1997).

Fig. 18. Deposition of low carbon steel over (a) copper and (b) aluminium substrates (Rao et al., 2012b).

Fig. 19. Plot of axial force and thermocouple measurements performed at the substrate bottom surface. FS of Stellite 6 over AISI 316. Initial deformation and deposition phases were both rod feed rate controlled (Vitanov et al., 2010).

Fig. 20. Evolution of FS variables with time in the deposition of AISI 1020 over AISI 1020. Initial deformation was controlled by consumable rod feed rate at 1 mm/s, using a 2500 rpm rotation during a 4 mm length consumption. Deposition was force controlled using a 5 kN force and a 7.5 mm/s travel speed (Gandra et al., 2011).

Fig. 21. Effect of axial force on coating cross section morphology and joining interface. FS of mild steel over mild steel. Consumable rods with a 10 mm diameter, using a 2500 rpm rotation speed and a 4.2 mm/s travel speed (Gandra et al., 2012).

Fig. 22. Effect of axial force on substrate heat affected zone depth. FS of stainless steel over mild steel (Kalken, 2001).

Fig. 23. Effect of rotation speed on coating surface roughness and width. FS of AISI H13 over mild steel. Consumable rod with a 18 mm diameter, force of 10 kN and a 4 mm/s travel speed (Rafi et al., 2010a).

Fig. 24. Effect of travel speed on (a) width coating and (b) thickness. FS of austenitic stainless steel AISI 310 on low carbon Steel, using 18 mm diameter consumable rods, a 10 kN force and a rotation speed of 800 rpm (Rafi et al., 2010b).

Fig. 25. Effect of travel speed on bonding shear strength in the deposition of (a) austenitic stainless steel AISI 310 (Rafi et al., 2010b), (b) hot work tool steel AISI H13 over mild steel substrates (Rafi et al., 2010a). Both investigations reported the use of 18 mm diameter consumable rods, a 10 kN force and a 800 rpm rotation speed.

Fig. 26. Main bending failure modes reported in the deposition of AISI H13 over mild steel: (a) coating and (b) interface (Rafi et al., 2010a).

Fig. 27. Effect of travel speed on deposit bainic microstructure. Deposition of mild steel over mild steel using a 3 kN force, a 4.2 mm/s travel speed and a 10 mm diameter consumable rod (Gandra et al., 2012).

Fig. 28. Effect of consumable rod diameter and travel speed on austenitising kinetics. (a) Analytical relationship between the time spent in austenization domain, the traverse speed and the rod diameter, (b) effect of distance from centre (dc) for a 32 mm diameter rod (here referred as mechtrode), (c) effect of rod diameter (Md) (Bedford et al., 2001).

Fig. 29. FS process parameters and variables.

Fig. 30. Physical model of coating rod in friction surfacing based on the quasi-liquid layer concept (Liu et al., 2008).

Fig. 31. Transferring process in the FS of AISI H13 over mild steel. (a) Condition of the consumable rod after friction surfacing, (b) end portion of a friction surfaced coating (Rafi et al., 2010a).

Fig. 32. Micro-element at friction interface (Liu et al., 2009).

Fig. 33. Comparison between measured and calculated values of the thermal field generated along a initial plasticizing stage of 37 seconds, using a 4000 N, a 1825 rpm rotation speed (Liu et al., 2009).

Fig. 34. Functional relationships between major process parameters and coating state variables in FS (Vitanov et al., 2000).

Fig. 35. FS bonding parameters. (a) bonding time definition, (b) influence of consumable rod diameter and travel speed on bonding time (Vitanov and Voutchkov, 2005).

Fig. 36. V_x/V_z response surface - first stage of FS optimization (Voutchkov et al., 2001).

Fig. 37. Geometric arrangements for FS (Nicholas, 1993).

Fig. 38. Examples of non-linear trajectories of FS applied to (a) aluminium alloy AA6082 and (b) mild steel.

Fig. 39. Effect of overlapping distance on the appearance of multilayer deposits. FS of AA5052 over AA2017 (Tokisue et al., 2006).

Fig. 40. Macrostructures of multilayer deposit for several overlapping distances. AA5052 over AA2017 (Tokisue et al., 2006).

Fig. 41. Cross section hardness profile of multilayer deposits of AA5052 over AA2017 (Tokisue et al., 2006).

Fig. 42. (a) Cross-section of a multi-track friction surfaced coating of AISI 440C over low carbon steel. Displaying satisfactory bonding between successive tracks of deposited material. (b) Picture of a bent multi-track coated specimen (Puli and Janaki Ram, 2012b).

Fig. 43. Build-up by FS. (a) Successive deposition, (b) Bulk produced from four overlapped passes, (c) Detail of final thickness achieved, (d) Milling into final geometry (Vilaça et al., 2012).

Fig. 44. Hardness profile for the non-reinforced multi-layer deposition sample. Base Material hardness (137 HV) and the rod (105 HV) (Gandra et al., 2013b).

Fig. 45. Continuous AA6082-T6 build-up by FS along a 3D helicoidally trajectory (Vilaça et al., 2012).

Fig. 46. Water based cooling in FS. (a) Underwater FS process in the deposition of stainless steel over mild steel (Beyer et al., 2003) and (b) Use of water spray cooling in the FS of AA6082 over AA2024 (Ravi, 2011).

Fig. 47. Deposition of low carbon steel friction over aluminium substrate using a start-up plate (Rao et al., 2012b).

Fig. 48. Production of cutting tools based on FS. (a) Channel milled in preparation for FS inlay, (b) FS process being applied, (c) as-deposited coating, (d) post-processing into desirable geometry, (e) finished product. FRICTEC Inc. (Svarka, 2010).

Fig. 49. Traditional heat treatment cycle of high speed steels and FS thermal cycle followed by traditional tempering (Bedford et al., 2001).

Fig. 50. Microstructures of Stellite6 coatings a) friction surfaced, b) gas tungsten arc (Rao et al., 2012a).

Fig. 51. Usable bond and undercut definition, as defined by Voutchkov et al. (Voutchkov et al., 2001).

Fig. 52. Repair of turbine blade tips by FS. (a) Cross section of a deposit onto a blade tip and (b) repaired blade (Bedford et al., 1995).

Fig. 53. Method of forming a trailing edge on a steam turbine blade. (a) Deposition configuration and (b) section view evidencing the finished part (Amos, 1993).

Fig. 54. FS of stainless Steel on a mild steel cylindrical part using a Tricept TR805 robot. (a) Setup and clamping system, (b) deposition, (c) cross section macrograph of coating (Beyer et al., 2003).

Fig. 55. Device for treating rails in-situ (Doughty et al., 2009).

Table captions

Table 1. Reported FS material combinations deposited over steel substrates.

Table 2. Reported FS material depositions over non-ferrous substrates.

Table 3. Successful combinations of FS parameters.

Table 4. Investigations reporting the production of composites by FS.